Title

The path from root input to mineral-associated soil carbon is dictated by habitat-specific microbial traits and soil moisture

Authors

Sokol, Noah W

Foley, Megan M

Blazewicz, Steven J

et al.

Publication Date

2024-06-01

DOI

10.1016/j.soilbio.2024.109367

Soil Biology and Biochemistry 193 (2024) 109367

Contents lists available at ScienceDirect

Soil Biology and Biochemistry

journal homepage: www.elsevier.com/locate/soilbio

The path from root input to mineral-associated soil carbon is dictated by habitat-specific microbial traits and soil moisture

Noah W. Sokol [a,*], Megan M. Foley [b], Steven J. Blazewicz [a], Amrita Bhattacharyya [c], Nicole DiDonato [d], Katerina Estera-Molina [a,e], Mary Firestone [e], Alex Greenlon [f], Bruce A. Hungate [b], Jeffrey Kimbrel [a], Jose Liquet [a], Marissa Lafler [a], Maxwell Marple [a], Peter S. Nico [f], Ljiljana Paša-Tolić [d], Eric Slessarev [g], Jennifer Pett-Ridge [a,h,i,**]

[a] Lawrence Livermore National Laboratory, Physical & Life Science Directorate, Livermore, CA, USA
[b] Northern Arizona University, Center for Ecosystem Science and Society, Flagstaff, AZ, USA
[c] University of San Francisco, Department of Chemistry, San Francisco, CA, USA
[d] Pacific Northwest National Laboratory, Environmental Molecular Sciences Laboratory, Richland, WA, USA
[e] University of California Berkeley, Department of Environmental Science, Policy, and Management, Berkeley, CA, USA
[f] Lawrence Berkeley National Laboratory, Earth and Environmental Sciences, Berkeley, CA, USA
[g] Yale University, Department of Ecology and Evolution, New Haven, CT, USA
[h] University of California Merced, Life & Environmental Sciences Department, Merced, CA, USA
[i] Innovative Genomics Institute, Berkeley, CA, USA

ARTICLE INFO

Keywords:
Soil carbon
Microbial traits
Mineral-associated organic carbon
Drought
Carbon cycle
Global change
Stable isotope probing

ABSTRACT

Soil microorganisms help transform plant inputs into mineral-associated soil organic carbon (SOC) – the largest and slowest-cycling pool of organic carbon on land. However, the microbial traits that influence this process are widely debated. While current theory and biogeochemical models have settled on carbon-use efficiency (CUE) and growth rate as positive predictors of mineral-associated SOC, empirical tests are sparse, with contradictory observations. Using ^{13}C-labeling of an annual grass (*Avena barbata*) under two moisture regimes, we found that microbial traits associated with formation of ^{13}C-mineral-associated SOC varied by soil habitat, as did active microbial taxa and SOC chemical composition. In the rhizosphere, bacterial-dominated communities with fast growth, high biomass, and high extracellular polymeric substance (EPS) production were positively associated with ^{13}C-mineral-associated SOC. In contrast, the detritusphere held communities dominated by fungi and more filamentous bacteria, and with greater exoenzyme activity; there, ^{13}C-mineral-associated SOC was associated with slower microbial growth and lower microbial biomass. CUE was a negative predictor of ^{13}C-mineral-associated SOC in both habitats. Using ^{13}C-quantitative stable isotope probing, we found that the majority of ^{13}C assimilation in the rhizosphere and detritusphere at week 12 of the experiment was performed by very few bacterial and fungal taxa (3–5% of the total taxa that assimilated ^{13}C). Several complementary chemical analyses (^{13}C-NMR, FTICR-MS, and STXM-NEXAFS) suggested that SOC in the rhizosphere had a more oxidized chemical signature, while SOC in the detritusphere had a less oxidized, more lignin-like chemical signature. Our findings challenge current theory by demonstrating that microbial traits linked with mineral-associated SOC are not universal, but vary with soil habitat and moisture conditions, and are shaped by a small number of active taxa. Emerging SOC models that explicitly reflect these interactions may better predict SOC storage, since climate change causes shifts in soil moisture regimes and the ratio of living versus decaying roots.

1. Introduction

Soil microorganisms shape the global carbon balance by influencing the formation and decomposition of soil organic carbon (SOC) – the largest actively-cycling carbon pool on land (Batjes, 2014). The majority of SOC exists in association with soil minerals ('mineral-associated

* Corresponding author.
** Corresponding author. Lawrence Livermore National Laboratory, Physical & Life Science Directorate, Livermore, CA, USA.
E-mail addresses: sokol1@llnl.gov (N.W. Sokol), pettridge2@llnl.gov (J. Pett-Ridge).

https://doi.org/10.1016/j.soilbio.2024.109367
Received 19 October 2023; Received in revised form 1 February 2024; Accepted 12 February 2024
Available online 20 February 2024

SOC'); in grassland soils, for instance, more than 70% of SOC is mineral-associated (Sokol et al., 2022b). Since mineral-associated SOC constitutes both the largest and slowest-cycling pool of organic C – and its dynamics are intimately shaped by microbial processes (Whalen et al., 2022) – considerable attention has focused on which microbial traits influence its formation and loss (Wieder et al., 2013; Malik et al., 2020; Sokol et al., 2022b; Tao et al., 2023). A more explicit understanding of how soil microbial traits influence mineral-associated SOC could substantively improve the accuracy of biogeochemical models under climate change scenarios (Wieder et al., 2013, 2014).

Decaying microbial residues – such as cell envelopes, proteins, and extracellular polymeric substances – are increasingly recognized as key ingredients of mineral-associated SOC, and can comprise 50% or more of the total pool (Ludwig et al., 2015; Kallenbach et al., 2016; Angst et al., 2021). Through the '*in vivo* microbial turnover pathway', plant C is microbially assimilated and transformed into various microbial biomolecules; when released, these compounds can associate with soil minerals to form 'microbially-derived' mineral-associated SOC (Liang et al., 2017). A dominant current hypothesis is that greater microbial carbon-use efficiency (CUE) and faster microbial growth should lead to greater microbial residue production, and thus greater accrual of microbial-derived, mineral-associated SOC (Cotrufo et al., 2013; Craig et al., 2022). Indeed, a recent global-scale metanalysis suggests microbial CUE is a major determinant of total SOC stocks (Tao et al., 2023).

The hypothesis that growth rate and CUE are positively related to mineral-associated SOC has gained traction, and is now represented in several 'microbial-explicit' biogeochemical models (Wieder et al., 2014; Kyker-Snowman et al., 2020). However, the few empirical studies that have directly tested this hypothesis on the mineral-associated SOC fraction have found mixed support. While in some cases greater microbial growth and CUE can lead to more mineral-associated SOC (Kallenbach et al., 2015, 2016), others studies suggest these relationships can be neutral or negative (Craig et al., 2022). These contradictory findings may be because microbial residues are not always the dominant constituent of mineral-associated SOC (Angst et al., 2021; Chang et al., 2024). Mineral-associated SOC can have a more 'plant-derived' signature in some contexts (Kramer et al., 2012; Sanderman et al., 2014; Angst et al., 2021), such as when complex plant C (e.g. lignin) is partially decomposed by microbial exoenzymes into simpler plant compounds, and does not pass through a microbial body before associating with soil minerals (known as the '*ex vivo* modification pathway' (Liang et al., 2017)). It is also possible that distinct microbial traits are associated with different sources of plant C input, or distinct environmental conditions, leading to different pathways of mineral-associated SOC formation (Sokol et al., 2022b; Whalen et al., 2022). Despite the clear relevance to current theory and microbial-explicit biogeochemical models, few if any studies to date directly linked microbial traits and taxa with the accrual of mineral-associated SOC from different plant inputs and in the different microbial habitats where SOC is formed.

Rhizodeposits and decaying root biomass ('litter') are the two primary yet contrasting plant C sources that form mineral-associated SOC (Rasse et al., 2005; Sokol et al., 2019a; Pett-Ridge et al., 2021). Rhizodeposits enter the soil from living roots, and consist of lower-molecular weight exudates (such as organic acids and sugars), as well as volatiles, fine root turnover, and mucilage (Cheng and Gershenson, 2007). In the zone surrounding living roots, these inputs support a dynamic microbial habitat known as the 'rhizosphere'. By contrast, decaying root litter inputs are more biochemically complex, generating a microbial habitat known as the 'detritusphere' (Jackson et al., 2017; Sokol et al., 2019a; Villarino et al., 2021). Differences in the biochemical composition, quantity, and rate of delivery of rhizodeposits versus root litter select for distinct active microbial communities that specialize on these different inputs (Nuccio et al., 2020, 2021). By extension, we might expect the distinct rhizosphere versus detritusphere microbial communities to express different traits related to C processing, leading to different relationships between traits and mineral-associated SOC accrual and chemical composition (Sokol et al., 2022b) (Fig. 1). As terrestrial ecosystems vary in the relative proportion of plant C that enters the rhizosphere versus the detritusphere, this may help explain prior inconsistent observations between traits like growth rate and CUE on mineral-associated SOC in different environmental contexts (Kallenbach et al., 2015, 2016; Craig et al., 2022). Different trait patterns in the rhizosphere and detritusphere may also be modulated by environmental conditions that constrain microbial trait expression. Altered soil moisture, for example, has an overriding effect on soil microbial community composition and function (Jansson and Hofmockel, 2020), and can impact the expression of traits like CUE and exoenzyme activity (Sokol et al., 2022a), likely influencing the accrual of mineral-associated SOC (Heckman et al., 2023).

We hypothesized that distinct microbial traits and taxa in the rhizosphere and detritusphere would be associated with different formation pathways of ^{13}C-mineral-associated SOC, and these relationships would be shaped by soil moisture (Fig. 1). We posited that lower-molecular weight rhizodeposits may be assimilated by a rhizosphere microbial community with higher growth rate, biomass yield, and carbon-use efficiency (CUE), and transform plant inputs to microbially-derived SOC primarily via the *in vivo* microbial turnover pathway. In contrast, we hypothesized that more biochemically complex root detrital compounds may be partially decomposed by a detritusphere microbial community with greater exoenzyme activity, but a lower growth rate, to form SOC with a more lignin-like signature via the *ex vivo* modification pathway. To test this, we conducted a ^{13}C-labeling experiment and measured which microbial traits and taxa influenced mineral-associated SOC accrual and chemistry in the rhizosphere and detritusphere of an annual grass (*Avena barbata*) in a semi-arid grassland soil. During the 12-week growth span of A. *barbata*, we compared the movement of ^{13}C-labeled rhizodeposits into rhizosphere microbial communities and ^{13}C-mineral-associated SOC, with the movement of ^{13}C-labeled root litter into detritusphere microbial communities and ^{13}C-mineral-associated SOC. We compared these C fluxes under 'normal' moisture (~16% gravimetric soil moisture) (Foley et al., 2023) and droughted soil conditions (~8% soil moisture) (Hoover and Rogers, 2016; Pendergrass et al., 2017). We then measured in the rhizosphere and detritusphere: (i) the accrual and chemical composition of ^{13}C-mineral-associated SOC, (ii) a suite of community-level microbial traits (i.e., microbial carbon-use efficiency, growth rate, biomass, extracellular polymeric substances, and extracellular enzyme potential), and (iii) taxon-specific microbial activity via ^{13}C quantitative stable isotope probing.

2. Materials and methods

2.1. Experimental design

We conducted a ^{13}C-labeling greenhouse tracer and soil moisture manipulation study, where we maintained planted and unplanted microcosms inside growth chambers for 12 weeks, to track *Avena barbata* rhizodeposits versus root detritus, respectively (Supp. Figs. S1–S3). Soil for the experiment was collected from 0 to 10 cm depth ('A' mineral horizon) below a stand of *A. barbata* at the University of California Hopland Research and Extension Center (39°00.106′N, 123°04.184′W), which is the traditional and ancestral territory of the Shóqowa people and the current Hopland Band of Pomo Indians. The site is a Mediterranean annual grassland ecosystem (MAT max/min = 23/7 C; MAP = 956 mm yr^{-1}), where *Avena* spp. is the dominant vegetation. The soil is classified as a Typic Haploxeralfs (or a Luvisol) of the Witherall-Squawrock complex; the soil pH is ~5.6, and contains 45% sand, 36% silt, and 19% clay (Foley et al., 2023). Initial C and N content were 2.2% and 0.24%, respectively.

After collection, roots were removed, and soil was passed through a 2-mm sieve and packed to field bulk density (1.21 g cm^{-3}) in rectangular acrylic microcosms (11.5 × 2.9 × 25.5 linear cm), as described

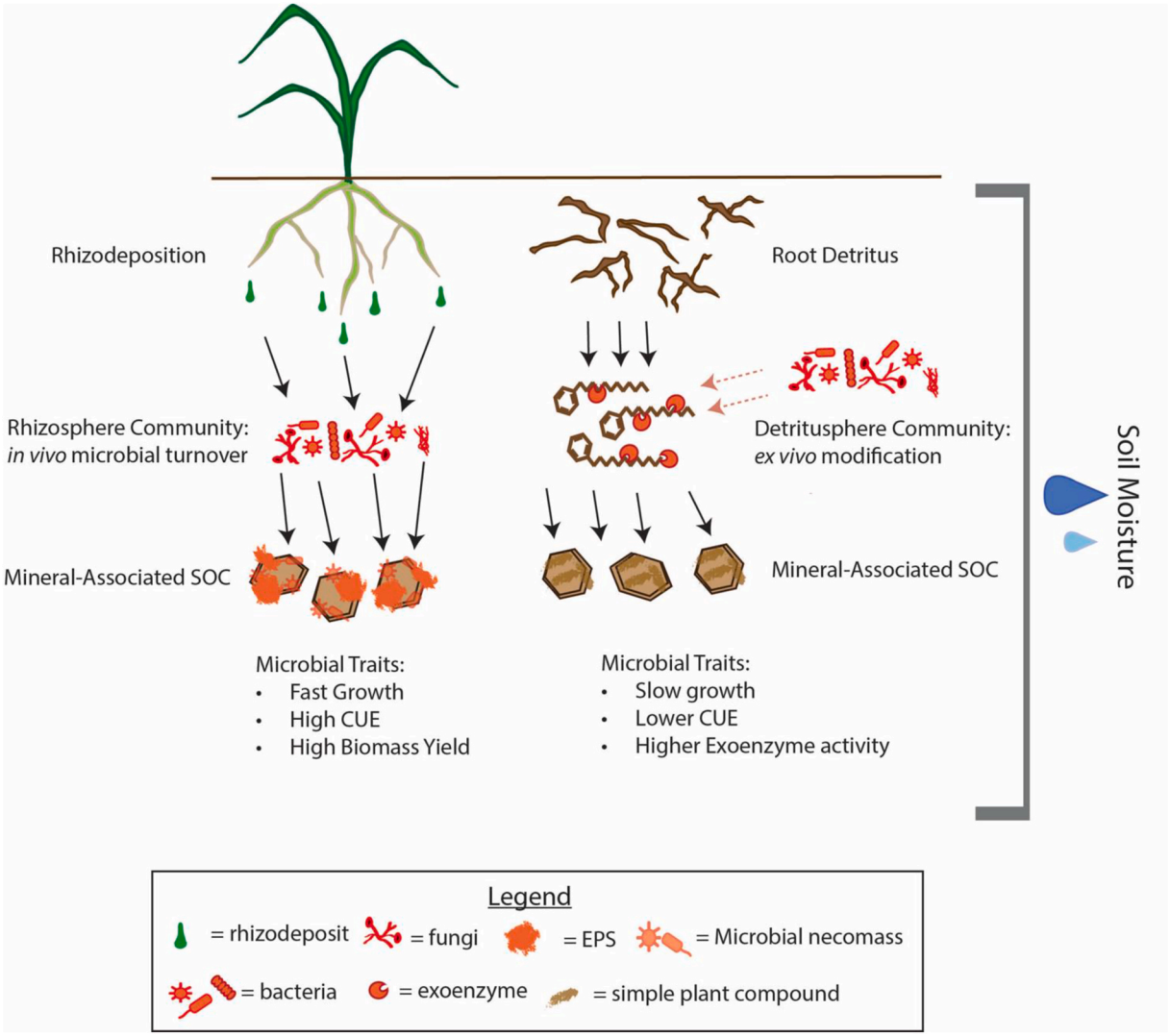

Fig. 1. Hypotheses on the role of habitat-specific microbial traits and soil moisture that shape the accrual of mineral-associated soil organic carbon (SOC). While contemporary theory posits that CUE and growth rate are positively associated with mineral-associated SOC, different plant carbon inputs (rhizodeposits vs. root detritus) may be associated with different habitat-specific microbial traits in the rhizosphere and detritusphere and different pathways of SOC formation. Lower-molecular weight rhizodeposits may be assimilated by a microbial community with higher growth rate, biomass yield, and carbon-use efficiency (CUE), and transform plant inputs to microbially-derived SOC via the *in vivo* microbial turnover pathway. In contrast, more biochemically complex root detrital compounds may be partially decomposed by a detritusphere microbial community with greater exoenzyme production, but a lower growth rate, to form SOC with a more lignin-like signature via the *ex vivo* modification pathway. Soil moisture – a master control variable – may exert a moderating influence on these patterns.

previously (Shi et al., 2015). For planted microcosms ('rhizodeposit' treatment), three germinated *Avena barbata* seedlings (collected from Hopland in spring 2018) were planted evenly apart in the soil, approximating a seedling density ~200 seedlings m^{-2} (i.e., within the range observed in the field) (Rai and Jain, 1982; Hallett et al., 2019). Microcosms were then incubated inside growth chambers (56 × 56 × 76 linear cm) at the Environmental Plant Isotope Chamber (EPIC) facility at the Oxford Tract Greenhouse at University of California Berkeley (Fig. S1) (Pett-Ridge and Firestone, 2017; Pett-Ridge et al., 2021). Chambers were maintained with a 16-h light period per day (from 6 a.m. to 10 p.m.), a maximum daytime and nighttime air temperature of 27 °C and 24 °C, respectively, and a CO_2 concentration between 400 and 450 ppm (specifics below). A subset of planted microcosms were grown inside $^{13}CO_2$ growth chambers, filled with ~99 atom% $^{13}CO_2$ (Sigma Aldrich), in order to track ^{13}C-labeled rhizodeposits into the rhizosphere ($n = 6$ per time point × moisture treatment combination; see Fig. S2). Plants were placed within the ^{13}C–CO_2 growth chambers for 10 continuous weeks of ^{13}C-labeling (following the initial 2-week seedling establishment phase). A control set of planted microcosms ($n = 4$) grown in $^{12}CO_2$ growth chambers (with a natural abundance atmosphere) was used for quantitative stable isotope probing (discussed below) and to increase available soil for measurements that did not require a ^{13}C-label (for example, exoenzyme activity) (Fig. S2).

$^{12}CO_2$ chambers were monitored using an Infrared Gas Analyzer (IRGA; SBA-5 CO_2 Gas Analyzer, PP systems, Amesbury, MA, USA) and $^{13}CO_2$ chambers were monitored using a Picarro G2201-I cavity ring-down spectrophotometer (Picarro Santa Clara, CA, USA). The entire system was controlled with a CR1000 datalogger (Campbell Scientific Logan, UT, USA). $^{12}CO_2$ and $^{13}CO_2$ chambers were monitored in parallel; each chamber was scanned once every 40 min to monitor CO_2 concentrations, and customized code (CRBasic) was developed to calculate the amount of CO_2 to add to each chamber, based on CO_2 drawdown and photosynthetically active radiation (PAR). Temperature was measured using Campbell Scientific 107 temperature probes (Campbell Scientific *107-U-L58-PT*, Logan, UT, USA) placed within each chamber. Probes were multiplexed into the labeling system using a Campbell Scientific AM16/32B Multiplexer (Campbell Scientific *AM16/32B-ST-SW*, Logan, UT, USA) that interfaced with the Campbell Scientific CR1000

Datalogger (Campbell Scientific *CR1000-ST-SW-NC*, Logan, UT, USA). The datalogger was programed to initiate cooling of chambers if the internal temperature was above 21 °C. Individual chambers were cooled using an internal radiator and fan system, with municipal water passing through Hayden 403 Oil Coolers (Aircraft Spruce, Corona, CA, USA). Computer fans placed behind the radiator system dissipated the cold air produced from the radiators into the rest of the chamber. Humidity/condensation was visually monitored every day within the chambers; condensation was minimized by wiping chambers down at the beginning of each morning before labeling began. The cooling system helped minimize condensation on the sides of the chambers during the day. Maintaining chambers at a set temperature also minimized transpiration, limiting condensation.

In unplanted microcosms (the 'root detritus' treatment), a 28-μm mesh 'detritusphere' bag was buried in the microcosm center, which contained ~65 g of Hopland soil mixed with 1–5 mm fragments of either ^{13}C-labeled or natural abundance *A. barbata* root detritus (0.013 g root detritus dry g soil^{-1}), to roughly simulate field concentrations of *A. barbata* root detritus (Nuccio et al., 2020) (Figs. S2–3). Prior studies have examined the decay of *Avena* spp. root detritus in this EPIC chamber facility and in the field, and found that the majority of mineralization of root detritus occurs during a single growing season, likely due to the relatively low C:N ratio and high decomposability of *Avena* root fragments (Bird et al., 2011; Shi et al., 2018; Nuccio et al., 2020; Fossum et al., 2022). To generate *A. barbata* root detritus, *A. barbata* plants (from the same supply of seeds as used in the main experiment) were grown for 7 weeks in a mix of sand and Hopland soil between March and April 2019 (i.e., immediately before the experimental period). After a two-week seedling establishment phase, plants were moved into the EPIC growth chambers. A subset of *A. barbata* plants were exposed to 5 weeks of continuous $^{13}CO_2$ labeling (similar protocol as described above), and a subset were grown in natural abundance $^{12}CO_2$ growth chambers. At the end of the growth period, roots were harvested and repeatedly washed, dried at room temperature until they reached constant mass, and then cut into 1–5 mm fragments, before being mixed with Hopland soil and packed into detritusphere bags. The % total C and δ^{13}C of root fragments was measured on an elemental analyzer coupled to an isotope ratio mass spectrometer (EA-IRMS; Costech ECS 4010, Costech Analytical Technologies, Valencia, CA, USA). The ^{13}C-enriched root detritus treatment (n = 6) contained ^{13}C-labeled root detritus (77 ± 1.7 atom% ^{13}C-labeled), while the natural abundance root detritus treatment (n = 4) contained natural abundance root detritus (1.1 atom% ^{13}C) (Fig. S2). All unplanted microcosms (i.e., both the ^{13}C-enriched and the natural abundance root detritus treatments) were incubated in growth chambers with a natural abundance CO_2 headspace throughout the experimental period.

Planted and unplanted microcosms were maintained at one of two moisture treatments, to simulate differences in soil moisture during the spring growing season in California semiarid grasslands: 'normal moisture' (~16% ± 0.3 gravimetric soil moisture; mean ± standard error) or 'spring drought' conditions (~8% ± 0.5 gravimetric soil moisture) (Foley et al., 2023). Soil moisture was monitored throughout the experimental period by weighing all microcosms twice weekly, and adjusting soil moisture by mass (Shi et al., 2015). At each harvest (4, 8, and 12 weeks), gravimetric soil moisture was measured for all microcosms (Fig. S4). We confirmed that the hydrological conditions of the detritusphere mesh bags were not significantly different from the rhizosphere (see ANOVA table below Fig. S3; p = 0.8), nor from the bulk soil surrounding the detritusphere mesh bags, by comparing these values in all detritusphere microcosms at week 12 (paired t-test, p = 0.4).

In total, the experiment contained 120 microcosms. Each combination of moisture (normal, drought) × harvest time point (4, 8, 12 weeks) × plant C input (rhizodeposits, root detritus) had 10 replicate microcosms (divided between: n = 6 ^{13}C-labeled and n = 4 natural abundance controls) (see Fig. S2 for full experimental design).

2.2. Sample collection

At each harvest, aboveground *A. barbata* biomass in planted microcosms was clipped at the base of the stems, dried at 65 °C and weighed. Rhizosphere soil was collected by gently shaking the root systems to remove loosely attached soil; soil still clinging to the roots was characterized as rhizosphere. A subset of roots + rhizosphere soil was immediately placed within a 15-mL falcon tube on dry ice and stored at −80 °C. The remaining rhizosphere soil was carefully separated from the roots by hand; a subset was kept fresh at room temperature for gravimetric soil moisture and other assays (described below), and a subset was air-dried for SOC analysis. In unplanted microcosms (root detritus treatment), detritusphere soil was collected from inside the 28-μm 'detritusphere mesh bag'; care was taken to avoid any visually apparent pieces of decaying root material. As above, subsets of soil were stored at −80 °C, fresh, and air-dried.

2.3. SOC analysis

We isolated the mineral-associated SOC fraction on all ^{13}C-labeled soils (n = 6) and a set of natural abundance samples from week 12 (n = 4), using a combined density and physical fractionation method (Soong and Cotrufo, 2015). We added 25 mL of 1.85 g cm^3 sodium polytungstate (SPT) to 5 g of air-dried soil in a 50-mL falcon tube. To disperse aggregates, samples were shaken on a reciprocal shaker (~200 oscillations/minute) for 18 h with glass beads. The supernatant was filtered with a glass fiber filter to separate the light particulate fraction (<1.85 g cm^{-3}). The pelletized heavy fraction at the base of the tube (<1.85 g cm^{-3}) was rinsed three times with deionized water to remove all excess SPT. The heavy fraction pellet was then vortexed with 25-mL deionized water and passed through a 53-μm sieve. This <53-μm fraction (clay + fine silt) was defined as mineral-associated SOC (Bradford et al., 2008; Soong and Cotrufo, 2015). Mineral-associated SOC samples were dried, ground, weighed, and analyzed for % total C and δ^{13}C on an elemental analyzer coupled to an isotope ratio mass spectrometer (EA-IRMS; Costech ECS 4010, Costech Analytical Technologies, Valencia, CA, USA). Atom% ^{13}C enrichment of mineral-associated SOC was calculated by subtracting atom% ^{13}C of mineral-associated SOC at t = 0 from the atom% ^{13}C in the enriched sample. The total μg of ^{13}C that accumulated in the mineral-associated SOC fraction was then calculated by multiplying %C of the mineral-associated SOC fraction by the atom % ^{13}C enrichment of the mineral-associated fraction at a given timepoint (4, 8, 12 weeks).

2.4. Microbial traits

Immediately after each harvest, we measured a suite of microbial traits on fresh soil, including microbial biomass C (MBC; including total MBC and ^{13}C-MBC), extracellular polymeric substances (EPS; including total EPS and ^{13}C-EPS), extracellular enzyme activity, and microbial community-level growth rate and carbon use efficiency (CUE). Microbial biomass C was measured via a chloroform fumigation extraction protocol on two ~3–6 g soil subsamples (Vance et al., 1987). One ~3–6g subsample was extracted in 25 mL of 0.05M K_2SO_4 immediately, and one ~3–6 g subsample was fumigated with chloroform prior to extraction in a sealed vacuum desiccator for 5 days (Bruulsema and Duxbury, 1996). Both extracts were filtered (Whatman No. 40) and analyzed for total C on a Shimadzu TOC Analyzer, and for δ^{13}C on a Thermo DeltaPlus XP GasBench. The unfumigated sample was defined as dissolved organic C (DOC); microbial biomass C (MBC) was calculated as the difference between the fumigated – unfumigated samples (extraction efficiency K_{EC} = 0.45) (Beck et al., 1997). Atom% ^{13}C enrichment of MBC was calculated according to the equation (Mehnaz et al., 2019; Husain et al., 2024):

$$^{13}C_{MBC} = (C_{fum} \times {}^{13}C_{fum} - C_{nonfum} \times {}^{13}C_{nonfum})/(C_{fum} - C_{nonfum})$$

$^{13}C_{MBC}$ is the atom% enrichment of MBC, C_{fum} and $^{13}C_{fum}$ are the

total C and atom%^{13}C of the fumigated extract, and C_{nonfum} and $^{13}C_{nonfum}$ is the %C and atom% ^{13}C of the non-fumigated extract.

To extract extracellular polymeric substances (EPS), we used a modified cation exchange resin extraction method (Redmile-Gordon et al., 2014; Wang et al., 2019) with an added ethanol precipitation step (for detailed method, see: Sher et al., 2020). Briefly, 5–10 g of soil was added to a cooled 50-mL falcon tube containing 15-mL of phosphate buffer saline and 2 g cation exchange resin (Dowex® Marathon® C, 20–50 mesh, Na^+ form, Sigma-Aldrich, St. Louis). Samples were vortexed, shaken, and centrifuged, and 8-mL of the supernatant was passed through a 0.2 μm nylon syringe filter. EPS was precipitated from the filtrate with three, 24-mL volumes of freezer-cold, 100% ethanol and concentrated 10×. The ethanol was dried off, and the pellet was resuspended in 0.5 mL of ultrapure MilliQ water. The extract was then transferred to a pre-weighed tin capsule, dried at 70 °C, and analyzed for %C and δ^{13}C using the same EA-IRMS as described above. Atom% ^{13}C enrichment of EPS was calculated by subtracting atom% ^{13}C in natural abundance control samples from atom% ^{13}C in enriched samples. The μg of ^{13}C-EPS g soil^{-1} was calculated by multiplying atom% ^{13}C enrichment by %C of the EPS, and dividing by the total g of soil from which EPS had been extracted (Sher et al., 2020).

We measured community-level CUE and mass-specific microbial growth rates using the substrate-independent, ^{18}O–H_2O method, which captures the incorporation of isotopically labeled water into microbial DNA (Spohn et al., 2016). The ^{18}O–H_2O method represents an improvement over prior, substrate-specific methods for measuring CUE, as it does not add energy rich substrate to the system and it does not rely on measuring the uptake of a single specific substrate, but captures how the microbial community processes the full suite of available C compounds – which is ideal for measuring broad differences in rhizodeposition vs root detritus. Importantly, this method does come with its own set of assumptions and potential biases – such as underestimating CUE relative to other methods, by assuming that all new oxygen in DNA is derived from extracellular water, capturing net growth instead of gross growth (Geyer et al., 2019; Pold et al., 2020), or potentially overestimating CUE in very dry soils (Canarini et al., 2020). These limitations are reviewed by Geyer et al. (2019) and Pold et al. (2020).

To measure CUE and growth rate, 1-g sample of fresh soil was weighed into a 20-mL Wheaton glass serum vial, and a total of 50-μL of water was added to each sample – a combination of ^{18}O–H_2O (98 atom % $H_2^{18}O$, Isoflex, San Francisco, CA, USA) and natural abundance H_2O – so the resulting soil water solution was ~20 atom% ^{18}O. An additional 1-g soil aliquot from a subset of 3 replicates from each moisture regime × microbial habitat combination at week 12 was incubated with 50-μL natural abundance water. We selected this volume of water after testing for the minimum amount of water that would ensure adequate diffusion throughout the sample, while also maintaining moisture differences between the two moisture treatments during the incubation period. Prior work suggests that, in grassland soils, adding roughly this volume of water to relatively dry soils should produce comparable results to the ^{18}O water vapor equilibration method (Canarini et al., 2020), and should allow for meaningful comparison between moisture treatments.

Vials were capped following the water addition. After a 72-h incubation at room temperature, 5-mL of gas from the vial headspace was collected for CO_2 analysis (and respiration rate) on a gas chromatograph (Agilent 7890B GC System). After sampling the headspace, the soil was removed and immediately flash frozen in liquid nitrogen and stored at −80 °C. DNA was extracted from frozen soil using a Qiagen DNEasy PowerSoil Pro kit; the bead beating step was performed for 1 min at 5.5 m^2/s on a FastPrep, all other manufacturer's instructions were followed. DNA was quantified using the Qubit DNA BR Assay Kit (ThermoFischer Scientific). A 50-μL aliquot of DNA was dried at 60 °C in a pre-weighed silver capsule spiked with 100 μL salmon sperm DNA (to achieve the oxygen detection limit) and analyzed for δ^{18}O and total O content (μg) on a Thermochemical Element Analyzer (TC/EA) coupled to an IRMS.

CUE and microbial growth rate were calculated from the amount of new DNA produced during the incubation period (tracked by ^{18}O incorporation into microbial DNA during growth). The amount of new DNA produced during the incubation period (DNA_p) is the difference in ^{18}O abundance between DNA from labeled and control incubations times the proportion (by mass) of DNA that is oxygen (0.3121) divided by the length of the incubation and mass of soil incubated. The conversion mass ratios of MBC:DNA for each sample was applied to calculate mass-specific growth rate (Gr) in mg C day^{-1} g^{-1} soil:

$$Gr = DNA_p \times \frac{MBC}{DNA}$$

where DNAp (μg DNA day^{-1} g^{-1} dry soil) is the DNA produced during the incubation, MBC (mg C g^{-1} dry soil) is microbial biomass C measured via chloroform fumigation extraction (described above), and DNA is the soil DNA concentration (μg DNA g^{-1} dry soil) determined via Qubit.

Carbon-use efficiency (CUE) was calculated as the amount of C used for growth relative to the sum of C allocated toward growth and respiration:

$$CUE = \frac{Gr}{Gr + Resp}$$

where Resp is the average respiration rate (mg C day^{-1} g^{-1} soil) during the incubation.

We measured extracellular enzymatic potential (nmol g^{-1} soil h^{-1}) of five different enzymes related to C-, N-, and P- cycling (see Table S7) using a fluorometric method (Kaiser et al., 2010). Briefly, 1.5 g of soil, which had been stored at −80 °C, was suspended in 150 mL of maleate buffer (25 mM, pH 4.95). 100 μL of soil suspension and 100 μL of substrate were pipetted into black microtiter plates, with five analytical replicates. Methylumbelliferyl (MUB) was used to calibrate all enzymes and a quench correction was performed. Plates were incubated in the dark at room temperature and fluorescence was measured every 30 min for 4 h at an excitation wavelength of 365 nm and an emission wavelength of 450 nm on a BioTek Synergy HT plate reader (Bio-Tek Instruments, Winooski, VT). Enzyme activity was calculated as the increase in fluorescence over time. Cumulative exoenzyme potential (nmol g^{-1} soil hr^{-1}) was calculated as the sum of average activity across all enzymes. The aim of this cumulative measurement was to estimate the total microbial investment in exoenzymes; as result, higher activity enzymes received proportionately higher weight when considering temporal dynamics and treatment effects.

2.5. Chemical composition of SOC

We used three complementary approaches to capture differences in the chemical composition of SOC formed in the rhizosphere and detritusphere at the final timepoint of the experiment (week 12): (i) Fourier transform ion cyclotron resonance mass spectrometry (FTICR-MS) provides molecular formulae with high-resolution for the whole water-extractable SOC pool (Fig. 6), considered a precursor to mineral-associated SOC (Kaiser and Kalbitz, 2012); (ii) ^{13}C-nuclear magnetic resonance (^{13}C-NMR) and (iii) scanning transmission X-ray microscopy in combination with near edge X-ray absorption fine structure spectroscopy (STXM-NEXAFS), which provide direct structural measurement of the carbon bond environments in mineral-associated SOC at the bulk and micro-scale, respectively (Figs. S7–S8).

2.5.1. Fourier transform ion cyclotron resonance mass spectrometer (FTICR-MS)

For each sample, 1 g of lyophilized soil was defrosted, added to a clean tube, and extracted with 2 mL Milli-Q water (<18.2 MΩ cm resistivity). The extraction was performed on 4 replicates ($n = 4$) for each treatment combination at the final timepoint (week 12). Samples were shaken at 1000 rpm at room temperature for 2 h using a vortex shaker,

centrifuged at 6000 rpm for 5 min, and the supernatant was removed. This was repeated with another 2 mL of Milli-Q water and supernatants were combined. Solid phase extraction (SPE) was performed on water extracts using Bond Elut PPL cartridges to remove salts and impurities that could interfere with MS analysis (Dittmar et al., 2008). Water extracts were diluted to 5 mL with Milli-Q water and adjusted to pH 2 with 2 μL of 85% H_3PO_4 prior to addition to methanol-activated PPL cartridges. Organic matter bound to the cartridges was rinsed with 50 mL of 10 mM HCl, dried with nitrogen and eluted in 1.5 mL of methanol.

Data was acquired using a 7 T Bruker ScimaX FTICR-MS operated with quadripolar (2×) detection and located in the Environmental Molecular Science Laboratory at Pacific Northwest National Laboratory (Richland, WA, USA). External calibration was performed using sodium trifluoracetic acid followed by shimming of the magnet to minimize 1× harmonic resonance peaks and tuning to optimize spectra for peak intensity, shape and resolution over the m/z range 200–1000. Extracts were direct infused into the electrospray source in negative ion mode at a voltage of +4 kV, temperature of 200 °C and dry gas flow of 4 L/min, in randomized order using a custom automated cart. Ion accumulation time was set to 10 ms and 2.1 s transients were coadded over 300 acquisitions in an 8 MW time domain for an estimated average resolution of ~680K at m/z 400. Internal recalibration of each spectrum, post-acquisition, was performed with calibration lists of standard OM components. Peak picking was performed in Data Analysis using a signal to noise ratio (S/N) threshold of 7, a relative intensity threshold of 0.01 and an absolute intensity threshold of 100,000.

Peak lists were exported and *Formularity* software (Tolić et al., 2017) was used to align spectra within a 0.5 ppm threshold and assign formulas using $N \leq 2$, $S = 0$ and $P = 0$, and <0.5 ppm error for high confidence assignments (average error <0.2 ppm). Peak lists were then corrected by subtracting peaks detected in extraction blanks. Elemental ratios were calculated from molecular formulas assigned for each peak and averaged for each sample. Molecular class distributions were based on percentage of formulas with elemental ratios within the H/C and O/C ranges for major compound classes (Kim et al., 2003; Tolić et al., 2017) present in each sample. Elemental classifications are putative yet provide a useful indication of the major chemical compound classes and allow for broad comparisons of formula types detected in each sample treatment.

2.5.2. Synchrotron-based scanning transmission X-ray microscopy (STXM) in combination with near edge X-ray absorption fine structure (NEXAFS) spectroscopy

STXM analysis was performed on the Molecular Environmental Sciences beamline 5.3.2.2 of the Advanced Light Source (ALS) at Lawrence Berkeley National Laboratory (Berkeley, California, USA) (Kilcoyne et al., 2003; Warwick et al., 2003). A single replicate of a soil sample from each moisture regime × microbial habitat combination at week 12 were suspended in Milli-Q (18.2 Ω) water and the suspension was dropcast onto Si_3N_4 windows (Silson Ltd.) with a micropipette and air-dried. Carbon NEXAFS spectra were collected for 3–5 regions of interest (ROIs) per treatment. Care was taken to avoid thick C areas to prevent overabsorption. Calibration was done for the C 1s edge of gaseous CO_2 at 292.74 and 294.96 eV (Ma et al., 1991). Spatial and spectral resolution during the measurements were 40–50 nm and 0.1 eV, respectively. Dwell time was set at 2 ms. Transmission images at energies below and at the relevant absorption edge energies were converted into optical density (OD) images [$OD = \ln(I_0/I)$, with I_0 being the incident photon flux and I, the transmitted flux]. Image sequences (or "stacks") acquired at multiple energies spanning 278–330 eV for the C 1s edge were used to extract NEXAFS spectra. Clear areas of the Si_3N_4 membrane were used to normalize the transmission signal obtained from analyzed ROIs. All STXM data processing was done using the IDL package aXis 2000 (Hitchcock, 2006). C NEXAFS spectra were normalized using the Athena software package for X-ray absorption spectroscopy (Ravel and Newville, 2005).

2.5.3. ^{13}C-nuclear magnetic resonance

The ^{13}C chemical composition of mineral associated SOC samples were determined via solid state ^1H–^{13}C cross-polarization magic angle spinning (CP/MAS) nuclear magnetic resonance (NMR), on a 300 MHz Bruker Neo spectrometer at Lawrence Livermore National Laboratory (Livermore, CA, USA), operating at a ^{13}C Larmor frequency of 75.71 MHz. For each plant C input × moisture treatment combination (harvested at week 12), spectra were collected on a composite sample generated from 6 replicates of ^{13}C-labeled samples (n = 6). Soil samples (1g) were packed in 4 mm ZrO_2 rotors and spun at 10 kHz. ^{13}C CP/MAS experiments were collected with a contact time of 1.5 ms and used spinal 64 for proton decoupling. Each spectra was collected for 100,000–150,000 scans with a recycle delay of 2 s. α-glycine was used as a standard for setting up the CP experiment and the isotropic shift of the carboxyl groups ($\delta_{iso} = -176.5$ ppm) in α-glycine was used as the external reference for the ^{13}C chemical shift scale. ^{13}C spectra were deconvoluted with gaussian line shapes to determine relative fractions (Preston, 2001) using the software dmfit (Massiot et al., 2002) (Fig. S8). The line widths were informed by the chemical shift regions described for each organic matter compound class: alkyl C (0–45 ppm), N-Alkyl (45–60 ppm), O Alkyl (60–95 ppm), Di-O-Alkyl (95–110 ppm), aryl (110–145 ppm), O-aryl (145–165 ppm), amide (165–190 ppm), and ketone (190–215 ppm) (Nelson and Baldock, 2005).

2.6. DNA extraction and quantitative stable isotope probing

To measure taxon-specific fungal and bacterial C assimilation of ^{13}C-rhizodeposits or ^{13}C-detritus at week 12, we used ^{13}C quantitative stable isotope probing (^{13}C-qSIP) (Hungate et al., 2015; Koch et al., 2018). DNA was extracted from rhizosphere and detritusphere soil using a Qiagen DNEasy PowerSoil Pro kit (following the manufacturer's instructions, as described above) on three separate 0.25 g aliquots per sample, which were then combined into a single replicate ($n = 4$ per treatment, though some treatments had an $n = 3$, due to insufficient material in some samples to extract adequate DNA for SIP processing). For quantitative stable isotope probing, 5 μg of DNA in 150 μL 1xTE was loaded into a 5.2 mL ultracentrifuge tube and mixed with 1.00 mL gradient buffer, and 4.60 mL CsCl stock (1.885 g mL^{-1}) with a final average density of 1.725–1.730 g mL^{-1}. Samples were spun in a Beckman Coulter Optima XE-90 ultracentrifuge using a VTi65.2 rotor at 176, 284 RCF_{avg} at 20 °C for 108 h. Automated sample fractionation was performed using Lawrence Livermore National Laboratory's high-throughput SIP ('HT-SIP') pipeline (Nuccio et al., 2022a), generating 22–200 μL fractions per sample. The density of each fraction was measured with a Reichart AR200 digital refractometer fitted with a prism covering to facilitate measurement from 5 μL (Buckley et al., 2007). DNA was purified and concentrated using a Hamilton Microlab Star liquid handling system programmed to automate glycogen/PEG precipitations (Neufeld et al., 2007). The DNA concentration of each fraction was quantified with a PicoGreen fluorescence assay (Invitrogen, Thermo Fisher) (Nuccio et al., 2022b).

From each microcosm, fractions within the density range 1.650–1.760 g mL^{-1} and unfractionated DNA were prepared for amplicon sequencing of ITS and 16S rRNA genes. Bacterial 16S rRNA gene copies were quantified using quantitative PCR and primers 515 F and 806 R (Apprill et al., 2015; Parada et al., 2016). PCR conditions for 16S rRNA gene quantification were 95 °C for 2 min followed by 20 cycles of 95 °C for 30°S, 64.5 °C for 30°S, and 72 °C for 1 min. A total of 511 fraction libraries were sequenced for the 16S and ITS rRNA region on an Illumina MiSeq at Northern Arizona University's Genetics Core Facility using a 300-cycle and 500-cycle v2 reagent kit, respectively. Fungal 18S rRNA gene copies were also quantified in each density fraction using primers 1380F and 1510R. PCR conditions for 18S rRNA gene quantification were 98 °C for 3 min followed by 40 cycles of 98 °C for 45 s, 60 °C for 45 s and 72 °C for 30 s. DNA fractions, and unfractionated DNA, were amplified for fungal ITS rRNA using primers ITS4F

and 5.8SF. The PCR conditions for ITS amplification were 95 °C for 6 min followed by 35 cycles of 95 °C for 15 s, 55 °C for 30 s, and 72 °C for 1 min.

Paired-end reads were filtered to remove phiX and other contaminants with bbduk v38.56 (default settings except k = 31 and hdist = 1) (Bushnell, 2014). Fastq files were then trimmed to retain nucleotides 5–140 for the 16S F/R amplicons, and 5–245/175 for the ITS F and R reads, respectively, filtered for quality (maxEE = 2, truncQ = 2) and used to generate amplicon sequence variants (ASVs) with DADA2 v1.20 and phyloseq v1.36 (McMurdie and Holmes, 2013; Callahan et al., 2016). Chimeric sequences were determined and removed using removeBimeraDenovo from DADA2. ASV taxonomy was determined using the RDP 16S rRNA gene database (training set 18) using RDP classifier v2.11, keeping classifications with greater than 50% confidence (Wang et al., 2007), and with the UNITE v8.3 database for ITS amplicons (Nilsson et al., 2019). An alignment and phylogenetic tree was built using MAFFT v7.490 and FastTree v2.1.10 (Price et al., 2010; Katoh and Standley, 2013).

Excess atom fraction (EAF) ^{13}C of bacterial and fungal DNA was quantified following the procedure described by Hungate et al. (2015) and Koch et al. (2018) with some modifications. The density of each bacterial and fungal taxon was calculated as a weighted average across the CsCl density gradient. We used qPCR-based 16S rRNA or 18S gene copy number to normalize the relative abundance of taxa in each density fraction to compute weighted average density. The difference in a taxon's weighted average density between natural abundance (^{12}C) and ^{13}C-labeled soils, as well as the taxon's GC content, was used to estimate the change in the molecular weight of DNA due to incorporation of the ^{13}C isotope, expressed as EAF ^{13}C. We computed estimates of EAF ^{13}C for each taxon at the level of individual ultracentrifuge tubes as the difference in a taxon's weighted average density in a ^{13}C tube minus its average weighted average density across all replicate natural abundance tubes. Preliminary analysis showed an effect of ultracentrifuge tube on estimates of weighted average density, which has previously been attributed to slight differences in the CsCl density gradients among ultracentrifuge tubes (Morrissey et al., 2017). We corrected this technical error following the approach described in Morrissey et al. (2017). Estimates of EAF ^{13}C were weighted by a taxon's relative abundance in each experimental soil.

To assess total bacterial and fungal relative abundance in both rhizosphere and detritusphere habitats at week 12, we quantified total 16S and 18S rRNA gene copies via quantitative PCR. We approximated cumulative bacterial and fungal ^{13}C assimilation at week 12 for each sample by summing abundance-weighted EAF ^{13}C values across all fungal or bacterial taxa within the sample, to assess differences in overall activity (Fig. 4). Then, to directly compare between the rhizosphere and detritusphere treatments (which received different amounts of ^{13}C), we calculated '^{13}C proportional assimilation' at week 12 —which is defined as the relative proportion of cumulative ^{13}C assimilation performed by individual fungal and bacterial amplicon sequence variants (ASVs) (Raczka et al., 2021) (Fig. 5). This standardized ^{13}C assimilation value allowed us to compare taxon-specific activity across rhizosphere and detritusphere treatments (which received different total amounts of ^{13}C) but does not represent rates of C assimilation in mass units (Stone et al., 2021). 'Top assimilators' for each treatment were defined by ranking families that assimilated ^{13}C at week 12 in order of their relative ^{13}C assimilation, and summing up the values of the top assimilators until we reached a threshold value of at least 50% of the taxa that assimilated ^{13}C. We characterized known traits of these top assimilators by literature searches.

2.7. Statistical analysis

All analyses were conducted in R version 4.2.1 (R Core Team, 2022). The effect of microbial habitat and moisture regime on microbial traits at week 12 were analyzed with two-way ANOVA (Table S2). In these analyses, we specifically analyzed microbial traits that did not employ the ^{13}C-label (i.e., growth rate, carbon-use efficiency, total microbial biomass C, extracellular enzyme potential), to allow direct comparisons between rhizosphere and detritusphere treatments, as these treatments received different amounts of total ^{13}C from rhizodeposits versus root inputs, respectively. Differences between means for microbial traits at week 12 (Fig. 2) were calculated using Tukey's HSD ($p < 0.05$).

We used multiple regression to analyze the effect of soil moisture and different microbial traits (growth rate, CUE, ^{13}C-microbial biomass C, ^{13}C-EPS, % soil moisture) on ^{13}C-mineral-associated SOC across all time points (Craig et al., 2022). For these models, we centered and standardized predictor variables (using a z-transformation) so the regression slopes and the significance levels of predictor variables could be compared to one another (Schielzeth, 2010; Craig et al., 2022). Multiple regression models were run separately for the rhizosphere and the detritusphere (Fig. 3). We also ran these multiple regression models for each individual time point in the rhizosphere and detritusphere (Table S3). All models were screened for normality of residuals (Shapiro-Wilk test) and heteroscedasticity of residuals (visual assessment of residual plots). For FTICR-MS data, means were compared between the rhizosphere and detritusphere within a given moisture treatment at week 12 using t-tests (Fig. 6). For ^{13}C-qSIP data, cumulative ^{13}C-assimilation at week 12 was compared between bacteria and fungi within each microbial habitat × moisture treatment using t-tests (Fig. 4).

3. Results

3.1. Microbial traits and mineral-associated SOC in the rhizosphere and detritusphere

We found different patterns of trait expression in the detritusphere relative to the rhizosphere, which were shaped by soil moisture (Fig. 2; Table S2). Under normal moisture conditions, at the end of the experiment (week 12), the detritusphere soil had on average ~58% greater cumulative exoenzyme activity relative to the rhizosphere soil (Fig. 2a; $p < 0.05$). In contrast, the rhizosphere microbial community had a significantly faster community-level growth rate (Fig. 2b), higher CUE (Fig. 2c) and greater microbial biomass C (Fig. 2d) than the detritusphere community ($p < 0.05$). However, under droughted conditions, rhizosphere microbial community-level growth rate and CUE were not significantly different from the detritusphere (Fig. 2b–c; $p > 0.05$), and the difference between rhizosphere and detritusphere microbial biomass C was significantly reduced (Fig. 2d).

There were notable differences in which microbial traits were predictors of ^{13}C-mineral-associated SOC in the rhizosphere and detritusphere across the three time points (Fig. 3). In the rhizosphere, ^{13}C-EPS was the strongest positive predictor of ^{13}C-mineral-associated SOC ($p < 0.001$). Microbial community-level growth rate ($p < 0.001$) was also a significant positive predictor of ^{13}C-mineral-associated SOC in the rhizosphere. In contrast, microbial community-level growth rate trended towards being a negative predictor of ^{13}C-mineral-associated SOC in the detritusphere ($p = 0.1$) and ^{13}C-EPS had a non-significant effect in the detritusphere ($p > 0.4$). CUE was a negative predictor of ^{13}C-mineral-associated SOC in both the rhizosphere and the detritusphere ($p < 0.05$); the size of the negative coefficient was more than two times as large in the detritusphere compared to the rhizosphere. Soil moisture was a positive predictor of mineral-associated SOC in both habitats ($p < 0.05$).

3.2. Microbial activity in the rhizosphere and detritusphere

Based on total 16S and 18S rRNA gene copies at week 12, bacteria were ~41% more abundant in the rhizosphere relative to the detritusphere, whereas fungi were ~65% more abundant in the detritusphere than the rhizosphere (Fig. S5). In the detritusphere at week 12, fungal ^{13}C assimilation was 80% greater than bacterial ^{13}C assimilation under

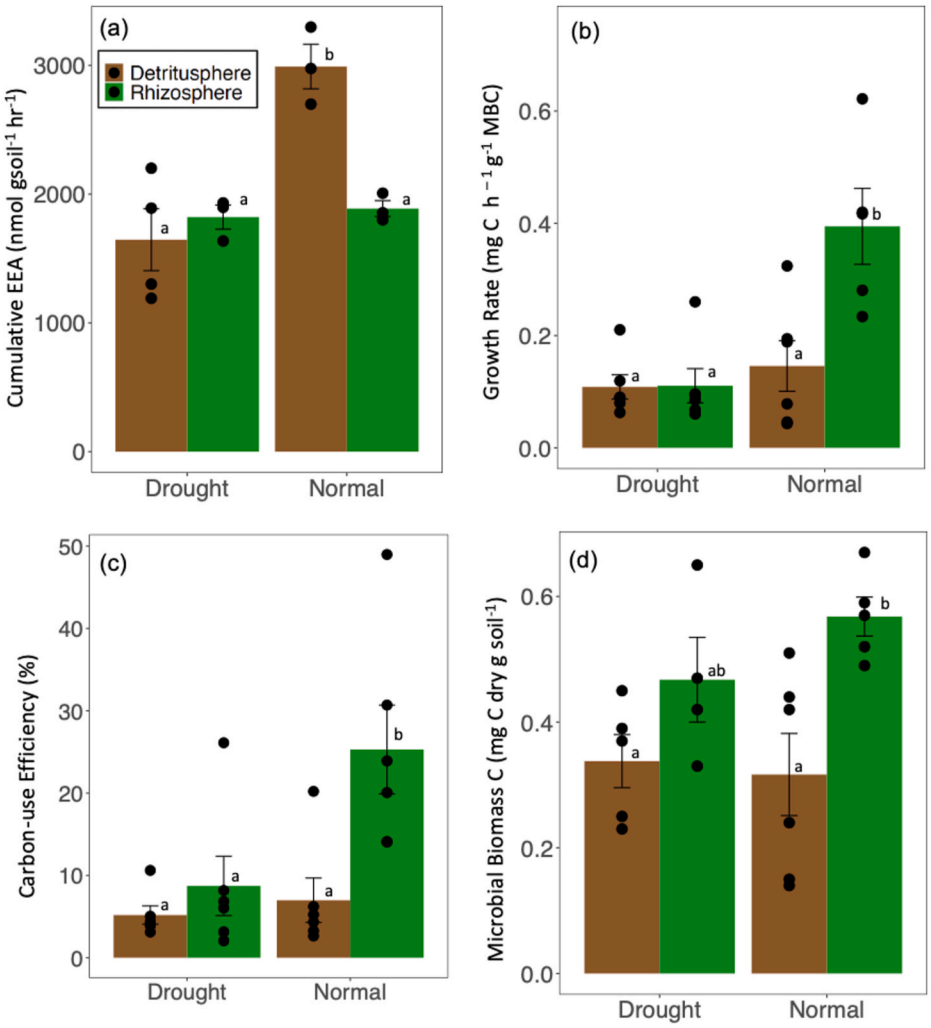

Fig. 2. Microbial traits in the detritusphere (brown bars) and rhizosphere (green bars) at the final experimental timepoint (12 weeks) of *Avena barbata* growth/incubation in a California annual grassland soil under normal moisture or droughted conditions. Microbial traits include: (a) cumulative exoenzyme activity (EEA; $n = 4$), (b) microbial community-level growth rate ($n = 6$), (c) microbial community-level carbon use efficiency (CUE; $n = 6$), and (d) microbial biomass carbon (MBC; $n = 6$). Letters indicate significant differences between means, determined via Tukey's HSD ($p < 0.05$). For full model output see Table S2.

normal moisture conditions and 46% greater under drought (Fig. 4b; $p < 0.05$). In contrast, in the rhizosphere at week 12, bacterial ^{13}C assimilation was 28% greater than fungal assimilation under normal moisture conditions (Fig. 4a; $p < 0.1$) and under droughted conditions, bacterial and fungal ^{13}C assimilation in the rhizosphere were not statistically different (Fig. 4a; $p > 0.1$).

In both the rhizosphere and detritusphere, a relatively small number of bacterial and fungal ASVs accounted for the majority of ^{13}C assimilation at week 12 (Fig. 5). Within each microbial habitat × moisture treatment, between 7 and 13 bacterial ASVs and 3–6 fungal ASVs accounted more than 50% of proportional ^{13}C-assimilation (defined as 'top assimilators'; see Methods) (Fig. S6; Table S4). These top bacterial assimilators represented only 3–4% of the total number of ^{13}C-active bacterial taxa at week 12 (i.e., bacterial ASVs that assimilated significant ^{13}C), and 0.6–1.6% of the total bacterial community detected at week 12 (Table S5). Likewise, the top fungal assimilators represented only 4–5% of all ^{13}C-active fungal taxa at week 12, and 0.7–1.7% of the total fungal community at week 12 (Table S5).

In the detritusphere, the top fungal assimilators include taxa from families in the Ascomycota (such as *Ceratostomataceae, Lasiosphaeriaceae,* and *Pleosporaceae)*. Top bacterial assimilators in the detritusphere included *Streptomycetaceae, Bacillaceae, Chitinophagaceae* (Fig. 5a). In the rhizosphere, top bacterial assimilators in soils with normal moisture conditions were from families in the Proteobacteria (*Comamonadaceae, Bradyrhizobiaceae*), Firmicutes (*Bacillaceae*), and Verrucomicrobia (*Spartobacteria*) (Fig. 5a). The top rhizosphere fungal assimilators were mostly saprotrophs, from the families *Aspergillaceae, Theloporaceae*, and *Piskurozymaceae, Hoehnelomycetaceae, and Pleosporaceae*.

There was notable overlap in the taxa that were top rhizosphere ^{13}C assimilators under drought and taxa that were top ^{13}C assimilators in the detritusphere at week 12 (regardless of soil moisture). For instance, filamentous *Streptomycetaceae* from the Actinobacteria were top assimilators in both the detritusphere and droughted rhizosphere soils, but were not top assimilators in the rhizosphere under normal moisture conditions (Fig. 5a; Table S4). In the droughted rhizosphere, several of the top fungal assimilators were also dominant in the detritusphere soils, including taxa from the families *Ceratostomataceae* and *Pleosporaceae* (Fig. 5b).

3.3. Chemical composition of SOC

All three methods used to characterize SOC chemical composition at week 12 indicated that SOC was more oxidized in the rhizosphere relative to the detritusphere. FTICR-MS showed that the water-extractable SOC fraction had a higher O:C ratio (Fig. 6a) and a higher

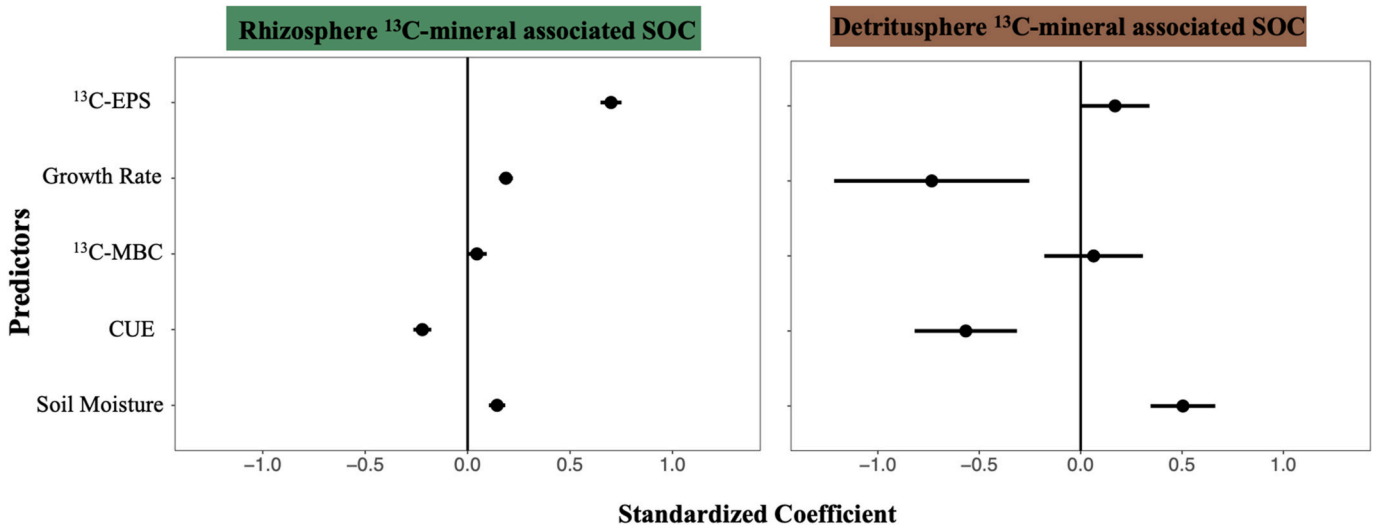

Fig. 3. Relationship between microbial traits and ^{13}C-mineral-associated SOC in the rhizosphere and detritusphere of *Avena barbata*. Coefficient plots with standardized regression coefficients (*z*-transformed) show the relationship between predictor variables (i.e., microbial traits and soil moisture) and ^{13}C-mineral-associated soil organic carbon (SOC; ug ^{13}C g soil $^{-1}$) in the (a) rhizosphere and (b) detritusphere of a California annual grassland soil across three time points (weeks 4, 8, 12). Microcosms were maintained under either normal moisture or droughted conditions over the 12-week experiment. Predictor variables include soil moisture and several microbial traits: ^{13}C-extracellular polymeric substances (^{13}C-EPS), microbial community-level growth rate ('growth rate'), ^{13}C-microbial biomass C (^{13}C-MBC, and microbial carbon-use efficiency (CUE). $N = 18$.

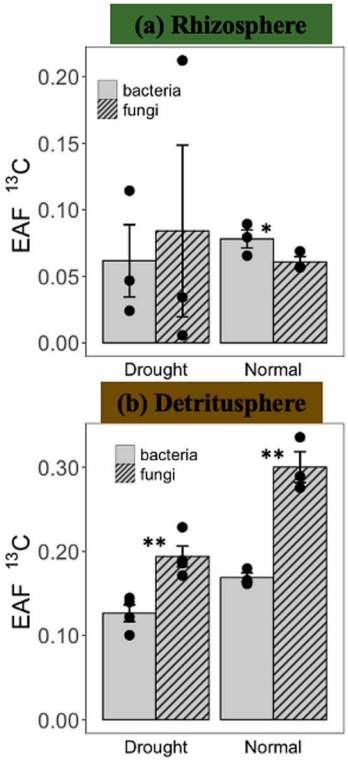

Fig. 4. Cumulative assimilation of ^{13}C-rhizodeposition or ^{13}C-detritus by bacteria and fungi in the (a) rhizosphere and (b) detritusphere of *Avena barbata* at 12 weeks of growth/incubation in a California annual grassland soil under normal moisture or droughted conditions, measured via ^{13}C-quantitative stable isotope probing. Cumulative excess atom fraction (EAF) ^{13}C represents the summed EAF ^{13}C values of all taxa, weighted by relative abundance. Asterisks indicate significant differences between means of bacterial and fungal cumulative EAF ^{13}C in each soil habitat × moisture treatment combination, measured via t-tests (*p ≤ 0.1, **p < 0.05). N = 3–4. Error bars indicate standard error.

nominal oxidation state of carbon (NOSC; Fig. S9) in the rhizosphere compared to the detritusphere under both normal moisture and drought conditions (*t*-test, p < 0.05). Likewise, the ^{13}C-NMR spectra of ^{13}C-mineral-associated SOC indicated a higher proportion of oxygenated C in the rhizosphere compared to the detritusphere, especially under normal moisture conditions, as indicated by the O-alkyl (60–95 ppm) and O-aryl (145–165 ppm) regions (Fig. S7; Table S6). STXM-NEXFAS data also corroborated these patterns. C NEXAFS spectra of rhizosphere mineral-associated SOC from the normal moisture treatment had a distinctive peak around 288.5 eV in the carboxyl region (Fig. S7) (Keiluweit et al., 2012). In contrast, the detritusphere mineral-associated SOC has a less oxidized profile, with no distinctive peak in the carboxyl region, but peaks in the 284.7 and 286.7 eV positions, in the aromatic C and phenolic C positions, respectively (Fig. S7) (Keiluweit et al., 2012). Under drought conditions, the C NEXAFS spectra of rhizosphere mineral-associated SOC appeared more similar to the detritusphere, as was observed with ^{13}C-NMR (Fig. S7).

FTICR-MS analysis indicated that under both normal moisture and drought conditions, the rhizosphere had a greater abundance of carbohydrate-like compounds (Fig. 6b), lipid-like compounds (Fig. 6c), protein-like compounds (Fig. 6d) and amino sugar-like compounds (Fig. 6e) relative to the detritusphere (t-tests, p < 0.05). ^{13}C-NMR spectra also revealed greater abundance of alkyl C in the rhizosphere (0–45 ppm) relative to the detritusphere, potentially indicative of long-chain lipids or other similar aliphatic compounds. In contrast, the detritusphere had a greater abundance of lignin-like compounds (Fig. 6f) – which may indicate less microbial processing of more complex plant C inputs (e.g., root litter).

4. Discussion

Soil microorganisms play a central role in the formation of SOC; both empirical and modeling efforts have sought to identify which microbial traits and taxa are linked with the accrual of mineral-associated SOC, especially under a changing climate (Wieder et al., 2013, 2014; Kallenbach et al., 2016; García-Palacios et al., 2021; Sokol et al., 2022a). Much of the effort to link microbial traits with SOC accrual has focused on community-level CUE and growth rate, because these traits are posited to be important in the formation of microbially-derived,

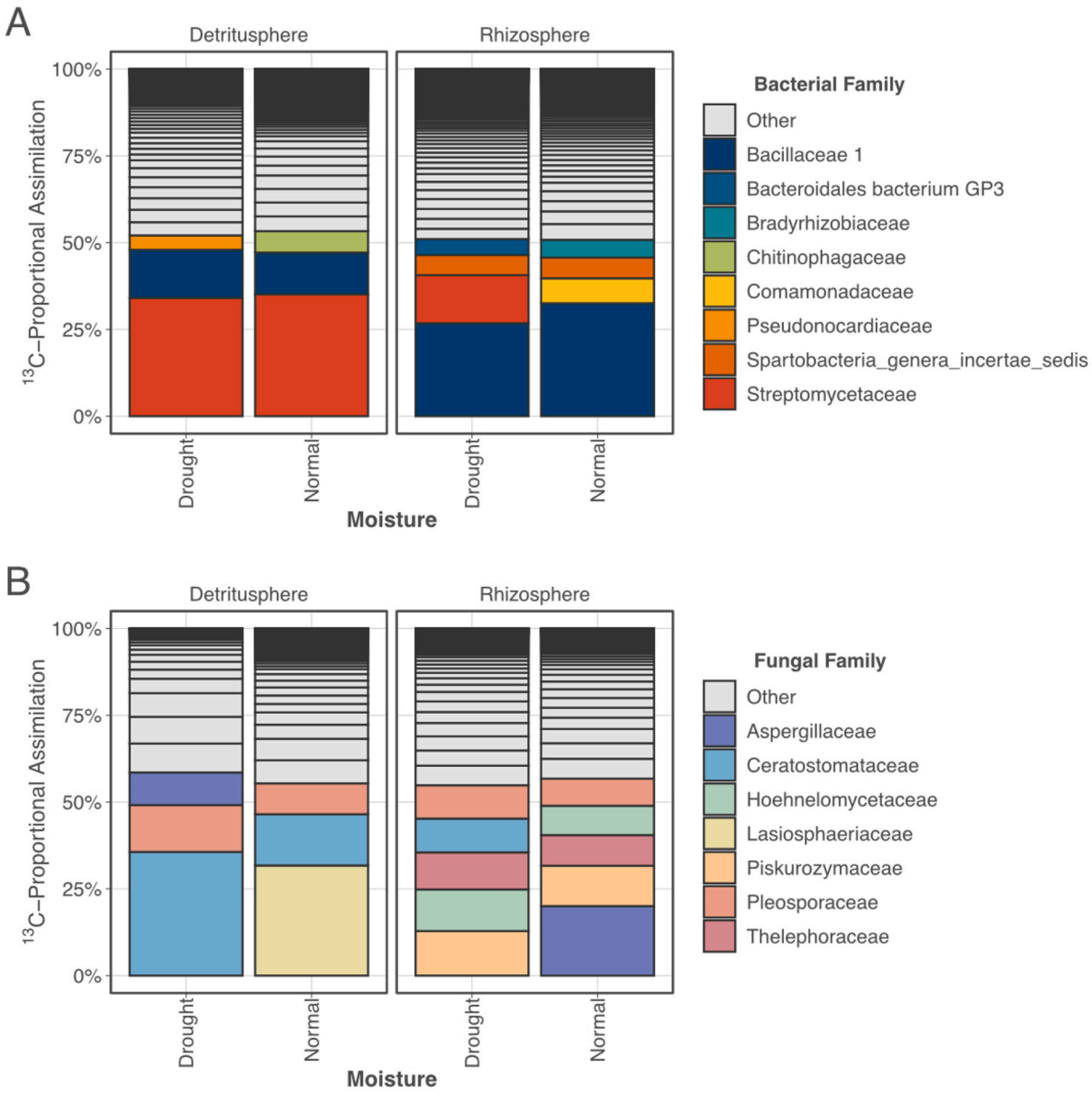

Fig. 5. Proportional ^{13}C assimilation of (a) bacterial and (b) fungal families in the rhizosphere and detritusphere of *Avena barbata* at 12 weeks, measured via ^{13}C-quantitative stable isotope probing. Measurements were taken after 12 weeks of growth/incubation in a California annual grassland soil under normal moisture (~16% soil moisture) or droughted conditions (~8% soil moisture). Bacterial and fungal taxa that together account for >50% of proportional ^{13}C assimilation (*i.e* 'top ^{13}C assimilators') are displayed in colored bars (see Methods, Table S4); all other active taxa are shown in greyscale bars. Bars indicate means, $n = 4$.

mineral-associated SOC that is formed from the residues of microorganisms that associate with soil minerals after cell death and turnover (Cotrufo et al., 2013; Wieder et al., 2014; Kallenbach et al., 2015, 2016). However, relatively few controlled studies have tested the role of these traits in different soil habitats or environmental contexts, or accounted for other pathways of SOC formation. For example, the partial decomposition of complex plant compounds by microbial exoenzymes into simpler plant compounds – which associate with minerals to form plant-derived SOC – may be associated with a different set of microbial traits (Fig. 1). Indeed, we found evidence that the two dominant and contrasting microbial habitats in soil – the rhizosphere and detritusphere – selected for different microbial traits, which mapped onto contrasting microbial life history strategies and pathways of mineral-associated SOC formation. Moreover, a small number of bacterial and fungal taxa accounted for the majority of ^{13}C-assimilation at the end of week 12 – specifically, only 3–5% of the active bacterial or fungal community (i.e. the taxa that assimilated ^{13}C) – suggesting a narrow range of taxa may be driving a disproportionate amount of the C transformations in soil at a given timepoint.

The rhizosphere of *A. barbata* selected for a microbial community with faster growth, higher biomass, and higher CUE relative to the detritusphere (Fig. 2). Together, these traits typify a microbial life history strategy specialized for environments with high availability of simple resources, like sugars and amino acids, which are more abundant in the rhizosphere. This life history strategy has been described recently as a 'high yield' strategy (Malik et al., 2020). Overall, we found that ^{13}C-EPS was the strongest positive predictor of ^{13}C-mineral-associated SOC in the rhizosphere (Fig. 2a). Growth rate, ^{13}C-MBC, and soil moisture were also positive predictors of ^{13}C-mineral-associated SOC in the rhizosphere (Fig. 3a). In the detritusphere, the dominant microbial traits and active taxa were different from those we identified in the rhizosphere. The more complex, polymeric root detrital compounds were

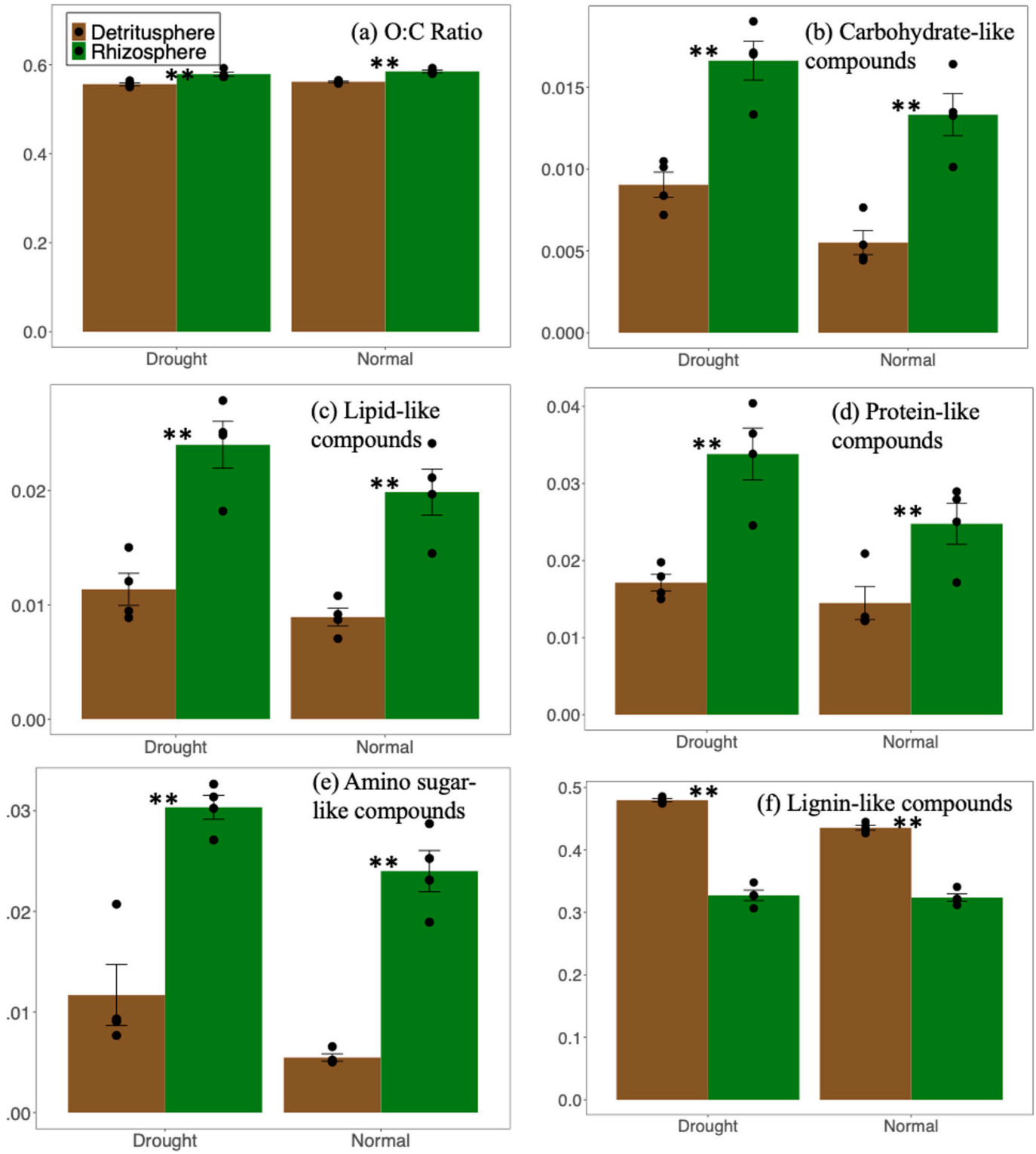

Fig. 6. Chemical composition of soil organic carbon (SOC) in the rhizosphere (green) and detritusphere (brown) of *Avena barbata* measured via FTICR-MS ($n = 4$) at 12 weeks of growth/incubation under normal moisture or droughted conditions. Results include: (a) average oxygen to carbon ratio (O:C ratio), (b) carbohydrate-like compounds, (c) lipid-like compounds, (d) protein-like compounds, (e) aminosugar-like compounds, and (f) lignin-like compounds. Compound classes were assigned based on elemental ratios (see Methods); *y*-axis units in panel (a) is 'average O:C ratio'; *y*-axis units for all other panels is 'average % of formulas.' An asterisk* indicates significantly different means ($p < 0.05$) based on t-tests.

processed by a microbial community with slower growth, lower biomass and CUE, and higher extracellular enzyme activity, relative to the rhizosphere (Fig. 2). This set of microbial traits has been characterized as part of a 'resource acquisition' life history strategy (Malik et al., 2020), where high extracellular enzyme activity trades-off with both fast and efficient growth (Malik et al., 2019).

While current theory predicts that CUE is a positive predictor of mineral-associated SOC (Cotrufo et al., 2013), we found that across all

three time points, CUE was a negative predictor of ^{13}C-mineral-associated SOC in both the detritusphere and the rhizosphere (Fig. 3). These findings align with recent research which suggests that CUE can be a negative predictor of mineral-associated SOC (Craig et al., 2022). In the detritusphere, we posit that a trade-off between extracellular enzyme activity and CUE – typified by the resource acquisition life history strategy – may explain why CUE was a negative predictor of ^{13}C-mineral-associated SOC. In the rhizosphere, it was more surprising to find that CUE was a negative predictor of ^{13}C-mineral-associated SOC, since microbial community-level growth rate was a positive predictor, and because microbial CUE and growth rate are often positively related to one another – though the CUE-growth rate relationship is complex (Lipson, 2015; Anthony et al., 2020). Physiological trade-offs can also occur between growth rate and CUE, through various mechanisms such as ATP spilling or protein synthesis costs (Russell and Cook, 1995; Molenaar et al., 2009; Kallenbach et al., 2016), leading to a negative relationship between these two traits. It is possible that such a trade-off occurred in the rhizosphere, though additional research is necessary to untangle the relationship between CUE, growth rate and SOC accrual in the rhizosphere.

Bacteria assimilated more ^{13}C than fungi under normal moisture conditions in the rhizosphere at week 12 (Fig. 4a). On average, bacteria grow faster than fungi in soil, and turnover rates of bacteria can be an order of magnitude faster than fungi (Rousk and Bååth, 2007, 2011). These differences may be even more pronounced in the rhizosphere, where rates of predation and turnover are high, potentially generating a large yield of microbial necromass (Clarholm, 1985; Sokol and Bradford, 2019). The greater activity of bacteria than fungi in the rhizosphere at week 12 therefore supported the 'high yield' traits we observed in this habitat (Fig. 2). Given the outsized role played by a small number of microbial taxa in assimilating ^{13}C (Fig. 5), we queried the functional traits of these top assimilators (grouped by family) through literature searches to explore potential relationships between microbial traits and mineral-associated SOC formation. *Bacillaceae*, *Bradyrhizobiaceae*, *Comamondaceae, and Spartobacteria* – particularly active families in the rhizosphere (Fig. 5a) – contain taxa known to be successful rhizosphere competitors, exhibiting traits like high rates of motility, secondary metabolite production, and production of antifungal compounds (Haas and Défago, 2005; Covelli et al., 2013; Mandic-Mulec et al., 2015).

In the detritusphere, ^{13}C-assimilation at week 12 was dominated by saprotrophic, filamentous fungi (particularly taxa from the families *Aspergillaceae, Ceratostomataceae, Lasiosphaeriaceae,* and *Pleosporaceae*), which have an average turnover time that is much longer than soil bacteria (as discussed above), and can also exude high quantities of extracellular enzymes to degrade complex organic matter in litter or SOC (Osono, 2007) (Fig. 5). Several recent studies have observed that fungal-dominated communities can have lower CUE than bacterial-dominated communities, likely due to a trade-off between allocation to extracellular enzymes and growth rate/CUE (Soares and Rousk, 2019; Ullah et al., 2021). Indeed, extracellular enzyme activity and growth rate are known to trade off in filamentous fungi (Zheng et al., 2020); several other studies have described such a trade-off between extracellular enzyme activity and growth rate and/or CUE (Malik et al., 2019; Domeignoz-Horta et al., 2020). Recent work has also shown that the presence of a complex C substrate can result in lower CUE in fungal-dominated communities (Husain et al., 2024), likely due to such a trade-off. We posit that this trade-off occurred in the more fungal-dominated community in the detritusphere, since growth rate and CUE were lower and extracellular enzyme activity was higher in the detritusphere relative to the rhizosphere (Fig. 2), and also because growth rate and CUE were both negative predictors of ^{13}C-mineral-associated SOC in the detritusphere (Fig. 3).

Drought selected for a microbial community in the rhizosphere that more closely resembled the detritusphere community – both in several of the traits microbial expressed, as well as the identity of several active taxa assimilating ^{13}C at week 12. Under drought conditions, the differences between the rhizosphere and detritusphere in terms of extracellular enzyme activity, growth rate, CUE, and microbial biomass at week 12 were almost entirely negated (Fig. 2a–c) or significantly reduced (Fig. 2d). Active taxa in the droughted rhizosphere at week 12 were also similar to those in the detritusphere, particularly filamentous fungi and filamentous bacteria (e.g. *Streptomycetaceae*) with lignocellulolytic capabilities (Allison et al., 2013; de Vries et al., 2018; Xie et al., 2021). This may have been due to greater root death and turnover under drought, or drought-induced shifts in the chemical composition of rhizodeposits (i.e., greater amounts of complex organic acids and other compounds) (Gargallo-Garriga et al., 2018), which can affect which taxa are active and the traits they express (Naylor and Coleman-Derr, 2018).

Several converging lines of chemical evidence – including FTICR-MS, ^{13}C-NMR, and STXM-NEXAFS – suggested distinctive features of rhizosphere versus detritusphere SOC. All three methods indicated that the chemical composition of SOC in the rhizosphere had a more oxidized signature relative to the detritusphere, and a greater nominal oxidation state of carbon (NOSC) (Fig. 6, Fig. S7, Fig. S9). FTICR-MS showed greater abundance of compounds resembling amino sugars, proteins, carbohydrates and lipids in the rhizosphere relative to the detritusphere (Fig. 6). These features can be considered indicative of more microbially-derived SOC (Whalen et al., 2022), suggesting that rhizosphere SOC may have been formed via microbial assimilation and transformation of simple plant C substrates into microbial biomass and residues, which then became associated with soil minerals (i.e., the '*in vivo* microbial turnover pathway' (Liang et al., 2017)). The chemical composition of SOC in the detritusphere had a less oxidized profile than the rhizosphere, and a greater abundance of lignin-like compounds (Fig. 6, Fig. S7). This chemical signature more clearly resembled partially decomposed plant litter, which had not been as thoroughly transformed by microorganisms (Sanderman et al., 2014; Sokol et al., 2019b). This may suggest that a greater proportion of SOC in the detritusphere was formed via partial decomposition of complex plant compounds into simpler plant compounds that directly associated with soil minerals (described as the '*ex vivo* modification pathway' (Liang et al., 2017)). Some chemical data (i.e., STXM-NEXAFS) suggested that soil moisture modulated these patterns, as mineral-associated SOC in the droughted rhizosphere more closely resembled the detritusphere (Fig. S7).

Viewed together, several pieces of complementary evidence (microbial traits, ^{13}C-qSIP, chemical composition of SOC via FTICR-MS, ^{13}C NMR, and STXM-NEXAFS) support our hypotheses that: (1) distinct pathways of mineral-associated SOC formation predominate in the rhizosphere versus the detritusphere of *A. barbata,* (2) these pathways are associated with distinct microbial traits and taxa, and (3) soil moisture can modulate these relationships (Fig. 1). The '*in vivo* microbial turnover pathway' may dominate in the rhizosphere of grasslands soils, where fast-growing taxa with high biomass yield thrive on lower-molecular weight plant inputs (e.g. certain root exudates). These substrates are biosynthesized into various intracellular and extracellular microbial compounds, which subsequently form SOC with a more microbially-derived signature relative to the detritusphere (Fig. 6; Fig. S7). Microbial traits like growth rate, biomass, and EPS may help predict mineral-associated SOC accrual in the rhizosphere, although relationships with CUE are more complex (Fig. 3). In contrast, in the detritusphere, microorganisms with fast growth and high yield may not be as competitive on more complex sources of organic C (e.g., root detritus), where greater exoenzyme activity is required to decompose these complex compounds into simpler compounds (Poll et al., 2008; Malik et al., 2019, 2020; Ramin and Allison, 2019; Zheng et al., 2020). The '*ex vivo* modification pathway' may dominate in the detritusphere of grassland soils, characterized by exoenzyme-mediated depolymerization of more complex inputs (i.e., root litter) into simpler plant compounds, which form mineral-associated SOC with a more lignin-like, 'plant-derived' signature (Fig. 6; Fig. S7). External forcings like drought can modulate these relationships, selecting for a rhizosphere microbial

community that behaved more like the detritusphere community in terms of which taxa were active in assimilating ^{13}C, some of the community-level traits expressed, as well as the formation of mineral-associated SOC via the *ex vivo* modification pathway.

Future research can build upon the findings presented in this study. First, there is a critical need to enhance existing methodological approaches and incorporate novel techniques for assessing a diverse array of microbial traits. Notably, all current CUE methods have limitations that hinder their accuracy, such as measuring net growth instead of gross growth, failing to account for allocation to extracellular products, as well as comparability challenges between approaches (Geyer et al., 2019). The $^{18}O–H_2O$ CUE method may introduce biases in different moisture treatments and soil habitats based on the rate of microbial mortality and DNA degradation; promisingly, a new ^{18}O water equilibration method may represent a viable avenue for estimating CUE under different moisture conditions (Canarini et al., 2020), though more work is needed to better constrain the range of parameters that influence CUE values under different environmental conditions (Pold et al., 2020). Second, innovative approaches should be used to untangle how microbial versus plant traits temporally affect SOC cycling in dynamic habitats like the rhizosphere, including under different environmental stressors. For instance, it is challenging to distinguish microbial versus plant contributions to ^{13}C-EPS, and accurately identify plant versus microbial contributions to SOC (Whalen et al., 2022). Third, to understand how the activity of different microbial taxa change over time, such as throughout the growing season or various stages of root detritus decay, methods like qSIP should be conducted at multiple time points (Blazewicz et al., 2020; Nicolas et al., 2023). Given the dynamic nature of microbial populations, conducting time-resolved qSIP measurements could help to more accurately capture the contributions of different populations to ^{13}C–SOC accrual. Using a holistic approach will contribute to a more nuanced understanding of the intricate processes governing soil microbial dynamics and their impact on carbon cycling in diverse ecosystems.

5. Conclusion

Our results challenge current hypotheses of a consistent, positive relationship between mineral-associated SOC and traits like CUE and growth rate (Bradford et al., 2013; Cotrufo et al., 2013), by demonstrating that these relationships are shaped by microbial habitat and soil moisture. While growth rate was a positive predictor of mineral-associated SOC in the rhizosphere, it was a negative predictor in the detritusphere; CUE was a negative predictor in both habitats. Our findings on the role of plant C input and soil habitat may help explain prior contrasting observations on the role of growth rate/CUE in mineral-associated SOC accrual (Kallenbach et al., 2015, 2016; Craig et al., 2022). Our results also suggest that it is important to consider how soil microorganisms allocate their C under different resource environments (e.g., the rhizosphere versus the detritusphere) and different climate stressors (e.g., drought) – such as to growth versus resource acquisition – and the downstream consequences for SOC cycling (Geyer et al., 2020; Craig et al., 2022). Together, our data provide support for soil biogeochemical models that more explicitly account for different microbial habitats (Sulman et al., 2014) and microbial life history strategies (Wieder et al., 2014), and provide evidence that distinct life history strategies can be linked with a highly constrained number of active taxa in different soil habitats. To advance ecological theory and microbial-explicit biogeochemical models, it will be critical to accurately depict which microbial traits are linked with SOC storage in the different soil habitats where it is formed, as the relative proportion of living and dead root inputs can shift under climate change due to shifts in vegetation or altered allocation patterns (Malik et al., 2020; Marschmann et al., 2022; Sokol et al., 2022a), with direct implications for the quantity, chemical composition, and long-term persistence of SOC (Sokol et al., 2022a,b; Heckman et al., 2023).

CRediT authorship contribution statement

Noah W. Sokol: Conceptualization, Data curation, Formal analysis, Investigation, Methodology, Visualization, Writing – original draft, Writing – review & editing. **Megan M. Foley:** Data curation, Formal analysis, Investigation, Methodology, Visualization, Writing – review & editing. **Steven J. Blazewicz:** Conceptualization, Funding acquisition, Investigation, Methodology, Project administration, Supervision, Visualization, Writing – review & editing. **Amrita Bhattacharyya:** Investigation, Visualization, Writing – review & editing. **Nicole DiDonato:** Data curation, Formal analysis, Writing – review & editing. **Katerina Estera-Molina:** Investigation, Methodology, Resources, Visualization, Writing – review & editing. **Mary Firestone:** Conceptualization, Investigation, Supervision, Writing – review & editing. **Alex Greenlon:** Investigation, Methodology. **Bruce A. Hungate:** Funding acquisition, Investigation, Methodology, Supervision, Writing – review & editing. **Jeffrey Kimbrel:** Data curation, Formal analysis, Software, Visualization, Writing – review & editing. **Jose Liquet:** Investigation. **Marissa Lafler:** Investigation. **Maxwell Marple:** Investigation, Writing – review & editing. **Peter S. Nico:** Formal analysis, Funding acquisition, Visualization, Writing – review & editing. **Ljiljana Paša-Tolić:** Formal analysis, Visualization. **Eric Slessarev:** Formal analysis, Investigation, Methodology, Writing – review & editing. **Jennifer Pett-Ridge:** Conceptualization, Formal analysis, Funding acquisition, Investigation, Methodology, Project administration, Supervision, Writing – review & editing.

Declaration of competing interest

The authors declare that they have no known competing financial interests or personal relationships that could have appeared to influence the work reported in this paper.

Data availability

Data will be made available on request.

Acknowledgements

We thank Gianna Marschmann, Ella Sieradzki, Rhona Stuart, Erin Nuccio, Gareth Trubl, Cynthia Jeanette-Mancilla, Melanie Rodriguez-Fuentes, Dinesh Adhikari, Laura Adame, Peter Weber, Rachel Neurath, David Sanchez, Nameer Baker, Sarah Roy, Ilexis Chu-Jacoby, Rachel Hestrin, Emily Kline, Christina Fossum, Mengting Yuan, Alexa Nicolas, Anne Kakouridis, Donald Herman, Craig See, and Aaron Chew for assistance with soil collection, greenhouse harvests and lab analyses; Tina Winstrom at the Oxford Tract Greenhouse at UC Berkeley where the experiment was conducted, and John Bailey and Allison Smith at the Hopland Research and Extension Center where soil was collected. We thank Brad Erkkila at the Yale Analytical and Stable Isotope Laboratory and Jamie Brown at Northern Arizona University for help with stable isotope analyses; Jessica Wollard for assistance with DNA extractions, Michaela Hayer for sequencing DNA samples and conducting quantitative PCR, and Christina Ramon for assistance preparing soil samples for isotope analysis. We also thank Harris Mason, April Sawvel, and Christoper Colla for assistance with ^{13}C-NMR at LLNL; and Whendee Silver, Summer Ahmed, and Heather Deng for assistance with the gas chromatograph at UC Berkeley. The LLNL Soil Microbiome SFA team provided valuable feedback on experimental design and data interpretation. This research was supported by the U.S. Department of Energy, Office of Biological and Environmental Research, Genomic Science Program 'Microbes Persist' Scientific Focus Area (#SCW1632) at Lawrence Livermore National Laboratory (LLNL) and subcontracts to Northern Arizona University, Lawrence Berkeley National Laboratory, Pacific Northwest National Laboratory, and the University of California, Berkeley. Work conducted at LLNL was conducted under the auspices of

the U.S. Department of Energy under Contract DE-AC52-07NA27344. Work performed at Lawrence Berkeley National Laboratory was funded under U.S. Department of Energy contract number DE-AC02-05CH11231. Work performed at the Environmental Molecular Sciences Laboratory – a U.S. Department of Energy Office of Science User Facility at Pacific Northwest National Laboratory – was sponsored by the Biological and Environmental Research program under Contract No. DE-AC05-76RL01830.

Appendix A. Supplementary data

Supplementary data to this article can be found online at https://doi.org/10.1016/j.soilbio.2024.109367.

References

Allison, S.D., Lu, Y., Weihe, C., Goulden, M.L., Martiny, A.C., Treseder, K.K., Martiny, J. B.H., 2013. Microbial abundance and composition influence litter decomposition response to environmental change. Ecology 94, 714–725. https://doi.org/10.1890/12-1243.1.

Angst, G., Mueller, K.E., Nierop, K.G.J., Simpson, M.J., 2021. Plant- or microbial-derived? A review on the molecular composition of stabilized soil organic matter. Soil Biology and Biochemistry 156, 108189. https://doi.org/10.1016/j.soilbio.2021.108189.

Anthony, M.A., Crowther, T.W., Maynard, D.S., van den Hoogen, J., Averill, C., 2020. Distinct assembly processes and microbial communities constrain soil organic carbon formation. One Earth 2, 349–360. https://doi.org/10.1016/j.oneear.2020.03.006.

Apprill, A., McNally, S., Parsons, R., Weber, L., 2015. Minor revision to V4 region SSU rRNA 806R gene primer greatly increases detection of SAR11 bacterioplankton. Aquatic Microbial Ecology 75, 129–137. https://doi.org/10.3354/ame01753.

Batjes, N.H., 2014. Total carbon and nitrogen in the soils of the world. European Journal of Soil Science 65, 10–21. https://doi.org/10.1111/ejss.12114_2.

Beck, T., Joergensen, R.G., Kandeler, E., Makeschin, F., Nuss, E., Oberholzer, H.R., Scheu, S., 1997. An inter-laboratory comparison of ten different ways of measuring soil microbial biomass C. Soil Biology and Biochemistry 29, 1023–1032. https://doi.org/10.1016/S0038-0717(97)00030-8.

Bird, J.A., Herman, D.J., Firestone, M.K., 2011. Rhizosphere priming of soil organic matter by bacterial groups in a grassland soil. Soil Biology and Biochemistry, Knowledge gaps in soil C and N interactions 43, 718–725. https://doi.org/10.1016/j.soilbio.2010.08.010.

Blazewicz, S.J., Hungate, B.A., Koch, B.J., Nuccio, E.E., Morrissey, E., Brodie, E.L., Schwartz, E., Pett-Ridge, J., Firestone, M.K., 2020. Taxon-specific microbial growth and mortality patterns reveal distinct temporal population responses to rewetting in a California grassland soil. The ISME Journal 14, 1520–1532. https://doi.org/10.1038/s41396-020-0617-3.

Bradford, M.A., Fierer, N., Reynolds, J.F., 2008. Soil carbon stocks in experimental mesocosms are dependent on the rate of labile carbon, nitrogen and phosphorus inputs to soils. Functional Ecology 22, 964–974. https://doi.org/10.1111/j.1365-2435.2008.01404.x.

Bradford, M.A., Keiser, A.D., Davies, C.A., Mersmann, C.A., Strickland, M.S., 2013. Empirical evidence that soil carbon formation from plant inputs is positively related to microbial growth. Biogeochemistry 113, 271–281. https://doi.org/10.1007/s10533-012-9822-0.

Bruulsema, T.W., Duxbury, J.M., 1996. Simultaneous measurement of soil microbial nitrogen, carbon, and carbon isotope ratio. Soil Science Society of America Journal 60, 1787–1791. https://doi.org/10.2136/sssaj1996.03615995006000060025x.

Buckley, D.H., Huangyutitham, V., Hsu, S.-F., Nelson, T.A., 2007. Stable isotope probing with 15N achieved by disentangling the effects of genome G+ C content and isotope enrichment on DNA density. Applied and Environmental Microbiology 73, 3189–3195. https://doi.org/10.1128/AEM.02609-06.

Bushnell, B., 2014. BBMap: A Fast, Accurate, Splice-Aware Aligner (No. LBNL-7065E). Lawrence Berkeley National Lab. (LBNL), Berkeley, CA (United States).

Callahan, B.J., McMurdie, P.J., Rosen, M.J., Han, A.W., Johnson, A.J.A., Holmes, S.P., 2016. DADA2: high-resolution sample inference from Illumina amplicon data. Nature Methods 13, 581–583. https://doi.org/10.1038/nmeth.3869.

Canarini, A., Wanek, W., Watzka, M., Sandén, T., Spiegel, H., Šantrůček, J., Schnecker, J., 2020. Quantifying microbial growth and carbon use efficiency in dry soil environments via 18O water vapor equilibration. Global Change Biology 26, 5333–5341. https://doi.org/10.1111/gcb.15168.

Chang, Y., Sokol, N.W., van Groenigen, K.J., Bradford, M.A., Ji, D., Crowther, T.W., Liang, C., Luo, Y., Kuzyakov, Y., Wang, J., Ding, F., 2024. A stoichiometric approach to estimate sources of mineral-associated soil organic matter. Global Change Biology 30, e17092. https://doi.org/10.1111/gcb.17092.

Cheng, W., Gershenson, A., 2007. Chapter 2 – carbon fluxes in the rhizosphere. In: Cardon, Z.G., Whitbeck, J.L. (Eds.), The Rhizosphere. Academic Press, Burlington, pp. 31–56. https://doi.org/10.1016/B978-012088775-0/50004-5.

Clarholm, M., 1985. Interactions of bacteria, protozoa and plants leading to mineralization of soil nitrogen. Soil Biology and Biochemistry 17, 181–187. https://doi.org/10.1016/0038-0717(85)90113-0.

Cotrufo, M.F., Wallenstein, M.D., Boot, C.M., Denef, K., Paul, E., 2013. The Microbial Efficiency-Matrix Stabilization (MEMS) framework integrates plant litter decomposition with soil organic matter stabilization: do labile plant inputs form stable soil organic matter? Global Change Biology 19, 988–995. https://doi.org/10.1111/gcb.12113.

Covelli, J.M., Althabegoiti, M.J., López, M.F., Lodeiro, A.R., 2013. Swarming motility in Bradyrhizobium japonicum. Research in Microbiology 164, 136–144. https://doi.org/10.1016/j.resmic.2012.10.014.

Craig, M.E., Geyer, K.M., Beidler, K.V., Brzostek, E.R., Frey, S.D., Stuart Grandy, A., Liang, C., Phillips, R.P., 2022. Fast-decaying plant litter enhances soil carbon in temperate forests but not through microbial physiological traits. Nature Communications 13, 1–10. https://doi.org/10.1038/s41467-022-28715-9.

de Vries, F.T., Griffiths, R.I., Bailey, M., Craig, H., Girlanda, M., Gweon, H.S., Hallin, S., Kaisermann, A., Keith, A.M., Kretzschmar, M., Lemanceau, P., Lumini, E., Mason, K. E., Oliver, A., Ostle, N., Prosser, J.I., Thion, C., Thomson, B., Bardgett, R.D., 2018. Soil bacterial networks are less stable under drought than fungal networks. Nature Communications 9, 3033. https://doi.org/10.1038/s41467-018-05516-7.

Dittmar, T., Koch, B., Hertkorn, N., Kattner, G., 2008. A simple and efficient method for the solid-phase extraction of dissolved organic matter (SPE-DOM) from seawater. Limnology and Oceanography: Methods 6, 230–235. https://doi.org/10.4319/lom.2008.6.230.

Domeignoz-Horta, L.A., Pold, G., Liu, X.-J.A., Frey, S.D., Melillo, J.M., DeAngelis, K.M., 2020. Microbial diversity drives carbon use efficiency in a model soil. Nature Communications 11, 3684. https://doi.org/10.1038/s41467-020-17502-z.

Foley, M.M., Blazewicz, S.J., McFarlane, K.J., Greenlon, A., Hayer, M., Kimbrel, J.A., Koch, B.J., Monsaint-Queeney, V.L., Morrison, K., Morrissey, E., Hungate, B.A., Pett-Ridge, J., 2023. Active populations and growth of soil microorganisms are framed by mean annual precipitation in three California annual grasslands. Soil Biology and Biochemistry 177, 108886. https://doi.org/10.1016/j.soilbio.2022.108886.

Fossum, C., Estera-Molina, K.Y., Yuan, M., Herman, D.J., Chu-Jacoby, I., Nico, P.S., Morrison, K.D., Pett-Ridge, J., Firestone, M.K., 2022. Belowground allocation and dynamics of recently fixed plant carbon in a California annual grassland. Soil Biology and Biochemistry 165, 108519. https://doi.org/10.1016/j.soilbio.2021.108519.

García-Palacios, P., Crowther, T.W., Dacal, M., Hartley, I.P., Reinsch, S., Rinnan, R., Rousk, J., van den Hoogen, J., Ye, J.-S., Bradford, M.A., 2021. Evidence for large microbial-mediated losses of soil carbon under anthropogenic warming. Nature Reviews Earth & Environment 2, 507–517. https://doi.org/10.1038/s43017-021-00178-4.

Gargallo-Garriga, A., Preece, C., Sardans, J., Oravec, M., Urban, O., Peñuelas, J., 2018. Root exudate metabolomes change under drought and show limited capacity for recovery. Scientific Reports 8, 12696. https://doi.org/10.1038/s41598-018-30150-0.

Geyer, K., Schnecker, J., Grandy, A.S., Richter, A., Frey, S., 2020. Assessing microbial residues in soil as a potential carbon sink and moderator of carbon use efficiency. Biogeochemistry 151, 237–249. https://doi.org/10.1007/s10533-020-00720-4.

Geyer, K.M., Dijkstra, P., Sinsabaugh, R., Frey, S.D., 2019. Clarifying the interpretation of carbon use efficiency in soil through methods comparison. Soil Biology and Biochemistry 128, 79–88. https://doi.org/10.1016/j.soilbio.2018.09.036.

Haas, D., Défago, G., 2005. Biological control of soil-borne pathogens by fluorescent pseudomonads. Nature Reviews Microbiology 3, 307–319. https://doi.org/10.1038/nrmicro1129.

Hallett, L.M., Shoemaker, L.G., White, C.T., Suding, K.N., 2019. Rainfall variability maintains grass-forb species coexistence. Ecology Letters 22, 1658–1667. https://doi.org/10.1111/ele.13341.

Heckman, K.A., Possinger, A.R., Badgley, B.D., Bowman, M.M., Gallo, A.C., Hatten, J.A., Nave, L.E., SanClements, M.D., Swanston, C.W., Weiglein, T.L., Wieder, W.R., Strahm, B.D., 2023. Moisture-driven divergence in mineral-associated soil carbon persistence. Proceedings of the National Academy of Sciences 120, e2210044120. https://doi.org/10.1073/pnas.2210044120.

Hitchcock, A., 2006. Analysis of X-Ray Images and Spectra, in: xAxis2000. McMaster University, Hamilton, ON, Canada. https://doi.org/10.1016/j.elspec.2023.147360.

Hoover, D.L., Rogers, B.M., 2016. Not all droughts are created equal: the impacts of interannual drought pattern and magnitude on grassland carbon cycling. Global Change Biology 22, 1809–1820. https://doi.org/10.1111/gcb.13161.

Hungate, B.A., Mau, R.L., Schwartz, E., Caporaso, J.G., Dijkstra, P., Gestel, N. van, Koch, B.J., Liu, C.M., McHugh, T.A., Marks, J.C., Morrissey, E.M., Price, L.B., 2015. Quantitative microbial ecology through stable isotope probing. Applied and Environmental Microbiology 81, 7570–7581. https://doi.org/10.1128/AEM.02280-15.

Husain, H., Keitel, C., Dijkstra, F.A., 2024. Fungi are more important than bacteria for soil carbon loss through priming effects and carbon protection through aggregation. Applied Soil Ecology 195, 105245. https://doi.org/10.1016/j.apsoil.2023.105245.

Jackson, R.B., Lajtha, K., Crow, S.E., Hugelius, G., Kramer, M.G., Piñeiro, G., 2017. The ecology of soil carbon: pools, vulnerabilities, and biotic and abiotic controls. Annual Review of Ecology Evolution and Systematics 48, 419–445. https://doi.org/10.1146/annurev-ecolsys-112414-054234.

Jansson, J.K., Hofmockel, K.S., 2020. Soil microbiomes and climate change. Nature Reviews Microbiology 18, 35–46. https://doi.org/10.1038/s41579-019-0265-7.

Kaiser, C., Koranda, M., Kitzler, B., Fuchslueger, L., Schnecker, J., Schweiger, P., Rasche, F., Zechmeister-Boltenstern, S., Sessitsch, A., Richter, A., 2010. Belowground carbon allocation by trees drives seasonal patterns of extracellular enzyme activities by altering microbial community composition in a beech forest soil. New Phytologist 187, 843–858. https://doi.org/10.1111/j.1469-8137.2010.03321.x.

Kaiser, K., Kalbitz, K., 2012. Cycling downwards – dissolved organic matter in soils. Soil Biology and Biochemistry 52, 29–32. https://doi.org/10.1016/j.soilbio.2012.04.002.

Kallenbach, C.M., Frey, S.D., Grandy, A.S., 2016. Direct evidence for microbial-derived soil organic matter formation and its ecophysiological controls. Nature Communications 7, 13630. https://doi.org/10.1038/ncomms13630.
Kallenbach, C.M., Grandy, A.S., Frey, S.D., Diefendorf, A.F., 2015. Microbial physiology and necromass regulate agricultural soil carbon accumulation. Soil Biology and Biochemistry 91, 279–290. https://doi.org/10.1016/j.soilbio.2015.09.005.
Katoh, K., Standley, D.M., 2013. MAFFT multiple sequence alignment software version 7: improvements in performance and usability. Molecular Biology and Evolution 30, 772–780. https://doi.org/10.1093/molbev/mst010.
Keiluweit, M., Bougoure, J.J., Zeglin, L.H., Myrold, D.D., Weber, P.K., Pett-Ridge, J., Kleber, M., Nico, P.S., 2012. Nano-scale investigation of the association of microbial nitrogen residues with iron (hydr)oxides in a forest soil O-horizon. Geochimica et Cosmochimica Acta 95, 213–226. https://doi.org/10.1016/j.gca.2012.07.001.
Kilcoyne, A.L.D., Tyliszczak, T., Steele, W.F., Fakra, S., Hitchcock, P., Franck, K., Anderson, E., Harteneck, B., Rightor, E.G., Mitchell, G.E., Hitchcock, A.P., Yang, L., Warwick, T., Ade, H., 2003. Interferometer-controlled scanning transmission X-ray microscopes at the advanced light source. Journal of Synchrotron Radiation 10, 125–136. https://doi.org/10.1107/S0909049502017739.
Kim, S., Kramer, R.W., Hatcher, P.G., 2003. Graphical method for analysis of ultrahigh-resolution broadband mass spectra of natural organic matter, the van krevelen diagram. Analytical Chemistry 75, 5336–5344. https://doi.org/10.1021/ac034415p.
Koch, B.J., McHugh, T.A., Hayer, M., Schwartz, E., Blazewicz, S.J., Dijkstra, P., Gestel, N., van Marks, J.C., Mau, R.L., Morrissey, E.M., Pett-Ridge, J., Hungate, B.A., 2018. Estimating taxon-specific population dynamics in diverse microbial communities. Ecosphere 9, e02090. https://doi.org/10.1002/ecs2.2090.
Kramer, M.G., Sanderman, J., Chadwick, O.A., Chorover, J., Vitousek, P.M., 2012. Long-term carbon storage through retention of dissolved aromatic acids by reactive particles in soil. Global Change Biology 18, 2594–2605. https://doi.org/10.1111/j.1365-2486.2012.02681.x.
Kyker-Snowman, E., Wieder, W.R., Frey, S.D., Grandy, A.S., 2020. Stoichiometrically coupled carbon and nitrogen cycling in the MIcrobial-MIneral Carbon Stabilization model version 1.0 (MIMICS-CN v1.0). Geoscientific Model Development 13, 4413–4434. https://doi.org/10.5194/gmd-13-4413-2020.
Liang, C., Schimel, J.P., Jastrow, J.D., 2017. The importance of anabolism in microbial control over soil carbon storage. Nature Microbiology 2, 1–6. https://doi.org/10.1038/nmicrobiol.2017.105.
Lipson, D.A., 2015. The complex relationship between microbial growth rate and yield and its implications for ecosystem processes. Frontiers in Microbiology 6. https://doi.org/10.3389/fmicb.2015.00615.
Ludwig, M., Achtenhagen, J., Miltner, A., Eckhardt, K.-U., Leinweber, P., Emmerling, C., Thiele-Bruhn, S., 2015. Microbial contribution to SOM quantity and quality in density fractions of temperate arable soils. Soil Biology and Biochemistry 81, 311–322. https://doi.org/10.1016/j.soilbio.2014.12.002.
Ma, Y., Chen, C.T., Meigs, G., Randall, K., Sette, F., 1991. High-resolution K-shell photoabsorption measurements of simple molecules. Physical Review A 44, 1848–1858. https://doi.org/10.1103/PhysRevA.44.1848.
Malik, A.A., Martiny, J.B.H., Brodie, E.L., Martiny, A.C., Treseder, K.K., Allison, S.D., 2020. Defining trait-based microbial strategies with consequences for soil carbon cycling under climate change. The ISME Journal 14, 1–9. https://doi.org/10.1038/s41396-019-0510-0.
Malik, A.A., Puissant, J., Goodall, T., Allison, S.D., Griffiths, R.I., 2019. Soil microbial communities with greater investment in resource acquisition have lower growth yield. Soil Biology and Biochemistry 132, 36–39. https://doi.org/10.1016/j.soilbio.2019.01.025.
Mandic-Mulec, I., Stefanic, P., van Elsas, J.D., 2015. Ecology of Bacillaceae. American Society for Microbiology 3. https://doi.org/10.1128/microbiolspec.TBS-0017-2013.
Marschmann, G.L., Tang, J., Zhalnina, K., Karaoz, U., Cho, H., Le, B., Pett-Ridge, J., Brodie, E.L., 2024. Life History Strategies and Niches of Soil Bacteria Emerge from Interacting Thermodynamic, Biophysical, and Metabolic Traits, pp. 1–13. https://doi.org/10.1038/s41564-023-01582-w.
Massiot, D., Fayon, F., Capron, M., King, I., Le Calvé, S., Alonso, B., Durand, J.-O., Bujoli, B., Gan, Z., Hoatson, G., 2002. Modelling one- and two-dimensional solid-state NMR spectra. Magnetic Resonance in Chemistry 40, 70–76. https://doi.org/10.1002/mrc.984.
McMurdie, P.J., Holmes, S., 2013. Phyloseq: an R package for reproducible interactive analysis and graphics of microbiome census data. PLoS One 8, e61217. https://doi.org/10.1371/journal.pone.0061217.
Mehnaz, K.R., Corneo, P.E., Keitel, C., Dijkstra, F.A., 2019. Carbon and phosphorus addition effects on microbial carbon use efficiency, soil organic matter priming, gross nitrogen mineralization and nitrous oxide emission from soil. Soil Biology and Biochemistry 134, 175–186. https://doi.org/10.1016/j.soilbio.2019.04.003.
Molenaar, D., van Berlo, R., de Ridder, D., Teusink, B., 2009. Shifts in growth strategies reflect tradeoffs in cellular economics. Molecular Systems Biology 5, 323. https://doi.org/10.1038/msb.2009.82.
Morrissey, E.M., Mau, R.L., Schwartz, E., McHugh, T.A., Dijkstra, P., Koch, B.J., Marks, J. C., Hungate, B.A., 2017. Bacterial carbon use plasticity, phylogenetic diversity and the priming of soil organic matter. The ISME Journal 11, 1890–1899. https://doi.org/10.1038/ismej.2017.43.
Naylor, D., Coleman-Derr, D., 2018. Drought stress and root-associated bacterial communities. Frontiers in Plant Science 8, 2223. https://doi.org/10.3389/fpls.2017.02223.
Nelson, P.N., Baldock, J.A., 2005. Estimating the molecular composition of a diverse range of natural organic materials from solid-state 13C NMR and elemental analyses. Biogeochemistry 72, 1–34. https://doi.org/10.1007/s10533-004-0076-3.
Neufeld, J.D., Vohra, J., Dumont, M.G., Lueders, T., Manefield, M., Friedrich, M.W., Murrell, J.C., 2007. DNA stable-isotope probing. Nature Protocols 2, 860–866. https://doi.org/10.1038/nprot.2007.109.
Nicolas, A.M., Sieradzki, E.T., Pett-Ridge, J., Banfield, J.F., Taga, M.E., Firestone, M.K., Blazewicz, S.J., 2023. A subset of viruses thrives following microbial resuscitation during rewetting of a seasonally dry California grassland soil. Nature Communications 14, 5835. https://doi.org/10.1038/s41467-023-40835-4.
Nilsson, R.H., Larsson, K.-H., Taylor, A.F.S., Bengtsson-Palme, J., Jeppesen, T.S., Schigel, D., Kennedy, P., Picard, K., Glöckner, F.O., Tedersoo, L., Saar, I., Kõljalg, U., Abarenkov, K., 2019. The UNITE database for molecular identification of fungi: handling dark taxa and parallel taxonomic classifications. Nucleic Acids Research 47, D259–D264. https://doi.org/10.1093/nar/gky1022.
Nuccio, E.E., Blazewicz, S.J., Lafler, M., Campbell, A.N., Kakouridis, A., Kimbrel, J.A., Wollard, J., Vyshenska, D., Riley, R., Tomatsu, A., Hestrin, R., Malmstrom, R.R., Firestone, M., Pett-Ridge, J., 2022a. HT-SIP: a semi-automated stable isotope probing pipeline identifies cross-kingdom interactions in the hyphosphere of arbuscular mycorrhizal fungi. Microbiome 10, 199. https://doi.org/10.1186/s40168-022-01391-z.
Nuccio, E.E., Blazewicz, S.J., Lafler, M., Campbell, A.N., Kakouridis, A., Kimbrel, J.A., Wollard, J., Vyshenska, D., Riley, R., Tomatsu, A., Hestrin, R., Malmstrom, R.R., Firestone, M., Pett-Ridge, J., 2022b. HT-SIP: A Semi-automated Stable Isotope Probing Pipeline Identifies Interactions in the Hyphosphere of Arbuscular Mycorrhizal Fungi. https://doi.org/10.1101/2022.07.01.498377.
Nuccio, E.E., Nguyen, N.H., Nunes da Rocha, U., Mayali, X., Bougoure, J., Weber, P.K., Brodie, E., Firestone, M., Pett-Ridge, J., 2021. Community RNA-Seq: multi-kingdom responses to living versus decaying roots in soil. ISME Communications 1, 1–10. https://doi.org/10.1038/s43705-021-00059-3.
Nuccio, E.E., Starr, E., Karaoz, U., Brodie, E.L., Zhou, J., Tringe, S.G., Malmstrom, R.R., Woyke, T., Banfield, J.F., Firestone, M.K., Pett-Ridge, J., 2020. Niche differentiation is spatially and temporally regulated in the rhizosphere. The ISME Journal 14, 999–1014. https://doi.org/10.1038/s41396-019-0582-x.
Osono, T., 2007. Ecology of ligninolytic fungi associated with leaf litter decomposition. Ecological Research 22, 955–974. https://doi.org/10.1007/s11284-007-0390-z.
Parada, A.E., Needham, D.M., Fuhrman, J.A., 2016. Every base matters: assessing small subunit rRNA primers for marine microbiomes with mock communities, time series and global field samples. Environmental Microbiology 18, 1403–1414. https://doi.org/10.1111/1462-2920.13023.
Pendergrass, A.G., Knutti, R., Lehner, F., Deser, C., Sanderson, B.M., 2017. Precipitation variability increases in a warmer climate. Scientific Reports 7, 17966. https://doi.org/10.1038/s41598-017-17966-y.
Pett-Ridge, J., Firestone, M.K., 2017. Using stable isotopes to explore root-microbe-mineral interactions in soil. Rhizosphere 3 3, 244–253. https://doi.org/10.1016/j.rhisph.2017.04.016.
Pett-Ridge, J., Shi, S., Estera-Molina, K., Nuccio, E., Yuan, M., Rijkers, R., Swenson, T., Zhalnina, K., Northen, T., Zhou, J., Firestone, M.K., 2021. Rhizosphere carbon turnover from cradle to grave: the role of microbe–plant interactions. In: Gupta, V.V. S.R., Sharma, A.K. (Eds.), Rhizosphere Biology: Interactions between Microbes and Plants, Rhizosphere Biology. Springer, Singapore, pp. 51–73. https://doi.org/10.1007/978-981-15-6125-2_2.
Pold, G., Domeignoz-Horta, L.A., DeAngelis, K.M., 2020. Heavy and wet: the consequences of violating assumptions of measuring soil microbial growth efficiency using the 18O water method. Elementa: Science of the Anthropocene 8, 69. https://doi.org/10.1525/elementa.069.
Poll, C., Marhan, S., Ingwersen, J., Kandeler, E., 2008. Dynamics of litter carbon turnover and microbial abundance in a rye detritusphere. Soil Biology and Biochemistry, Special Section: Functional Microbial Ecology: Molecular Approaches to Microbial Ecology and Microbial Habitats 40, 1306–1321. https://doi.org/10.1016/j.soilbio.2007.04.002.
Preston, C.M., 2001. Carbon-13 solid-state NMR of soil organic matter - using the technique effectively. Canadian Journal of Soil Science 81, 255–270. https://doi.org/10.4141/S00-074.
Price, M.N., Dehal, P.S., Arkin, A.P., 2010. FastTree 2 – approximately maximum-likelihood trees for large alignments. PLoS One 5, e9490. https://doi.org/10.1371/journal.pone.0009490.
Raczka, N.C., Piñeiro, J., Tfaily, M.M., Chu, R.K., Lipton, M.S., Pasa-Tolic, L., Morrissey, E., Brzostek, E., 2021. Interactions between microbial diversity and substrate chemistry determine the fate of carbon in soil. Scientific Reports 11, 19320. https://doi.org/10.1038/s41598-021-97942-9.
Rai, K.N., Jain, S.K., 1982. Population biology of Avena. Oecologia 53, 399–405. https://doi.org/10.1007/BF00389021.
Ramin, K.I., Allison, S.D., 2019. Bacterial tradeoffs in growth rate and extracellular enzymes. Frontiers in Microbiology 10. https://doi.org/10.1007/BF00389021.
Rasse, D.P., Rumpel, C., Dignac, M.-F., 2005. Is soil carbon mostly root carbon? Mechanisms for a specific stabilisation. Plant and Soil 269, 341–356. https://doi.org/10.1007/s11104-004-0907-y.
Ravel, B., Newville, M., 2005. ATHENA, ARTEMIS, HEPHAESTUS: data analysis for X-ray absorption spectroscopy using IFEFFIT. Journal of Synchrotron Radiation 12, 537–541. https://doi.org/10.1107/S0909049505012719.
Redmile-Gordon, M.A., Brookes, P.C., Evershed, R.P., Goulding, K.W.T., Hirsch, P.R., 2014. Measuring the soil-microbial interface: extraction of extracellular polymeric substances (EPS) from soil biofilms. Soil Biology and Biochemistry 72, 163–171. https://doi.org/10.1016/j.soilbio.2014.01.025.
Rousk, J., Bååth, E., 2011. Growth of saprotrophic fungi and bacteria in soil: growth of saprotrophic fungi and bacteria in soil. FEMS Microbiology Ecology 78, 17–30. https://doi.org/10.1111/j.1574-6941.2011.01106.x.

Rousk, J., Bååth, E., 2007. Fungal and bacterial growth in soil with plant materials of different C/N ratios. FEMS Microbiology Ecology 62, 258–267. https://doi.org/10.1111/j.1574-6941.2007.00398.x.

Russell, J., Cook, G., 1995. Energetics of bacterial growth: balance of anabolic and catabolic reactions. Microbiological Reviews 59, 48–62. https://doi.org/10.1128/mr.59.1.48-62.1995.

Sanderman, J., Maddern, T., Baldock, J., 2014. Similar composition but differential stability of mineral retained organic matter across four classes of clay minerals. Biogeochemistry 121, 409–424. https://doi.org/10.1007/s10533-014-0009-8.

Schielzeth, H., 2010. Simple means to improve the interpretability of regression coefficients: *Interpretation of regression coefficients*. Methods in Ecology and Evolution 1, 103–113. https://doi.org/10.1111/j.2041-210X.2010.00012.x.

Sher, Y., Baker, N.R., Herman, D., Fossum, C., Hale, L., Zhang, X., Nuccio, E., Saha, M., Zhou, J., Pett-Ridge, J., Firestone, M., 2020. Microbial extracellular polysaccharide production and aggregate stability controlled by switchgrass (Panicum virgatum) root biomass and soil water potential. Soil Biology and Biochemistry 143, 107742. https://doi.org/10.1016/j.soilbio.2020.107742.

Shi, S., Herman, D.J., He, Z., Pett-Ridge, J., Wu, L., Zhou, J., Firestone, M.K., 2018. Plant roots alter microbial functional genes supporting root litter decomposition. Soil Biology and Biochemistry 127, 90–99. https://doi.org/10.1016/j.soilbio.2018.09.013.

Shi, S., Nuccio, E., Herman, D.J., Rijkers, R., Estera, K., Li, J., da Rocha, U.N., He, Z., Pett-Ridge, J., Brodie, E.L., Zhou, J., Firestone, M., 2015. Successional trajectories of rhizosphere bacterial communities over consecutive seasons. mBio 6, e00746. https://doi.org/10.1128/mBio.00746-15.

Soares, M., Rousk, J., 2019. Microbial growth and carbon use efficiency in soil: links to fungal-bacterial dominance, SOC-quality and stoichiometry. Soil Biology and Biochemistry 131, 195–205. https://doi.org/10.1016/j.soilbio.2019.01.010.

Sokol, N.W., Bradford, M.A., 2019. Microbial formation of stable soil carbon is more efficient from belowground than aboveground input. Nature Geoscience 12, 46–53. https://doi.org/10.1038/s41561-018-0258-6.

Sokol, N.W., Kuebbing, S.E., Karlsen-Ayala, E., Bradford, M.A., 2019a. Evidence for the primacy of living root inputs, not root or shoot litter, in forming soil organic carbon. New Phytologist 221, 233–246. https://doi.org/10.1111/nph.15361.

Sokol, N.W., Sanderman, J., Bradford, M.A., 2019b. Pathways of mineral-associated soil organic matter formation: integrating the role of plant carbon source, chemistry, and point of entry. Global Change Biology 25, 12–24. https://doi.org/10.1111/gcb.14482.

Sokol, N.W., Slessarev, E., Marschmann, G.L., Nicolas, A., Blazewicz, S.J., Brodie, E.L., Firestone, M.K., Foley, M.M., Hestrin, R., Hungate, B.A., Koch, B.J., Stone, B.W., Sullivan, M.B., Zablocki, O., Pett-Ridge, J., 2022b. Life and death in the soil microbiome: how ecological processes influence biogeochemistry. Nature Reviews Microbiology 1–16. https://doi.org/10.1038/s41579-022-00695-z.

Sokol, N.W., Whalen, E.D., Jilling, A., Kallenbach, C., Pett-Ridge, J., Georgiou, K., 2022a. Global distribution, formation and fate of mineral-associated soil organic matter under a changing climate: a trait-based perspective. Functional Ecology. https://doi.org/10.1111/1365-2435.14040.

Soong, J.L., Cotrufo, M.F., 2015. Annual burning of a tallgrass prairie inhibits C and N cycling in soil, increasing recalcitrant pyrogenic organic matter storage while reducing N availability. Global Change Biology 21, 2321–2333. https://doi.org/10.1111/gcb.12832.

Spohn, M., Pötsch, E.M., Eichorst, S.A., Woebken, D., Wanek, W., Richter, A., 2016. Soil microbial carbon use efficiency and biomass turnover in a long-term fertilization experiment in a temperate grassland. Soil Biology and Biochemistry 97, 168–175. https://doi.org/10.1016/j.soilbio.2016.03.008.

Stone, B.W., Li, J., Koch, B.J., Blazewicz, S.J., Dijkstra, P., Hayer, M., Hofmockel, K.S., Liu, X.-J.A., Mau, R.L., Morrissey, E.M., Pett-Ridge, J., Schwartz, E., Hungate, B.A., 2021. Nutrients cause consolidation of soil carbon flux to small proportion of bacterial community. Nature Communications 12, 3381. https://doi.org/10.1038/s41467-021-23676-x.

Sulman, B.N., Phillips, R.P., Oishi, A.C., Shevliakova, E., Pacala, S.W., 2014. Microbe-driven turnover offsets mineral-mediated storage of soil carbon under elevated CO2. Nature Climate Change 4, 1099–1102. https://doi.org/10.1038/nclimate2436.

Tao, F., Huang, Y., Hungate, B.A., Manzoni, S., Frey, S.D., Schmidt, M.W.I., Reichstein, M., Carvalhais, N., Ciais, P., Jiang, L., Lehmann, J., Wang, Y.-P., Houlton, B.Z., Ahrens, B., Mishra, U., Hugelius, G., Hocking, T.D., Lu, X., Shi, Z., Viatkin, K., Vargas, R., Yigini, Y., Omuto, C., Malik, A.A., Peralta, G., Cuevas-Corona, R., Di Paolo, L.E., Luotto, I., Liao, C., Liang, Y.-S., Saynes, V.S., Huang, X., Luo, Y., 2023. Microbial carbon use efficiency promotes global soil carbon storage. Nature 618, 981–985. https://doi.org/10.1038/s41586-023-06042-3.

Tolić, N., Liu, Y., Liyu, A., Shen, Y., Tfaily, M.M., Kujawinski, E.B., Longnecker, K., Kuo, L.-J., Robinson, E.W., Paša-Tolić, L., Hess, N.J., 2017. Formularity: software for automated formula assignment of natural and other organic matter from ultrahigh-resolution mass spectra. Analytical Chemistry 89, 12659–12665. https://doi.org/10.1021/acs.analchem.7b03318.

Ullah, M.R., Carrillo, Y., Dijkstra, F.A., 2021. Drought-induced and seasonal variation in carbon use efficiency is associated with fungi:bacteria ratio and enzyme production in a grassland ecosystem. Soil Biology and Biochemistry 155, 108159. https://doi.org/10.1016/j.soilbio.2021.108159.

Vance, E.D., Brookes, P.C., Jenkinson, D.S., 1987. An extraction method for measuring soil microbial biomass C. Soil Biology and Biochemistry 19, 703–707. https://doi.org/10.1016/0038-0717(87)90052-6.

Villarino, S.H., Pinto, P., Jackson, R.B., Piñeiro, G., 2021. Plant rhizodeposition: a key factor for soil organic matter formation in stable fractions. Science Advances 7, eabd3176. https://doi.org/10.1126/sciadv.abd3176.

Wang, Q., Garrity, G.M., Tiedje, J.M., Cole, J.R., 2007. Naive Bayesian classifier for rapid assignment of rRNA sequences into the new bacterial taxonomy. Applied and Environmental Microbiology 73, 5261–5267. https://doi.org/10.1128/AEM.00062-07.

Wang, S., Redmile-Gordon, M., Mortimer, M., Cai, P., Wu, Y., Peacock, C.L., Gao, C., Huang, Q., 2019. Extraction of extracellular polymeric substances (EPS) from red soils (Ultisols). Soil Biology and Biochemistry 135, 283–285.

Warwick, T., Ade, H., Fakra, S., Gilles, M., Hitchcock, A., Kilcoyne, D., Shuh, D., Tyliszczak, T., 2003. Further Development of Soft X-Ray Scanning Microscopy with an Elliptical Undulator at the Advanced Light Source. Synchrotron Radiat. News 16, 22–27.

Whalen, E.D., Grandy, A.S., Sokol, N.W., Keiluweit, M., Ernakovich, J., Smith, R.G., Frey, S.D., 2022. Clarifying the evidence for microbial- and plant-derived soil organic matter, and the path toward a more quantitative understanding. Global Change Biology 28, 7167–7185. https://doi.org/10.1111/gcb.16413.

Wieder, W.R., Bonan, G.B., Allison, S.D., 2013. Global soil carbon projections are improved by modelling microbial processes. Nature Climate Change 3, 909–912. https://doi.org/10.1038/nclimate1951.

Wieder, W.R., Grandy, A.S., Kallenbach, C.M., Bonan, G.B., 2014. Integrating microbial physiology and physio-chemical principles in soils with the MIcrobial-MIneral Carbon Stabilization (MIMICS) model. Biogeosciences 11, 3899–3917. https://doi.org/10.5194/bg-11-3899-2014.

Xie, J., Dawwam, G.E., Sehim, A.E., Li, X., Wu, J., Chen, S., Zhang, D., 2021. Drought stress triggers shifts in the root microbial community and alters functional categories in the microbial gene pool. Frontiers in Microbiology 12. https://doi.org/10.3389/fmicb.2021.744897.

Zheng, W., Lehmann, A., Ryo, M., Vályi, K.K., Rillig, M.C., 2020. Growth rate trades off with enzymatic investment in soil filamentous fungi. Scientific Reports 10, 11013. https://doi.org/10.1038/s41598-020-68099-8.